Progress in Aerospace Sciences 44 (2008) 349–377

Contents lists available at ScienceDirect

Progress in Aerospace Sciences

journal homepage: www.elsevier.com/locate/paerosci

Hybrid LES/RANS methods for the simulation of turbulent flows

Jochen Fröhlich *, Dominic von Terzi [1]

Institut für Strömungsmechanik, Technische Universität Dresden, George-Bähr-Strasse 3c, 01062 Dresden, Germany

A B S T R A C T

The coupling of large eddy simulation (LES) with statistical turbulence models, i.e. Reynolds-Averaged Navier–Stokes (RANS) models, is arguably the main strategy to drastically reduce computational cost for making LES affordable in a wide range of complex industrial applications. The present paper presents a coherent review of the various approaches proposed in the recent literature on this topic. First, basic concepts and principal strategies highlighting the underlying ideas are introduced. This culminates in a general scheme to classify hybrid LES/RANS approaches. Following the structure of this novel classification, a larger number of individual methods are then described and assessed. Key methods are discussed in greater detail and illustrated with examples from the literature or by own results. The aim of the review is to provide information on how to distinguish different methods and their ingredients and to further the understanding of inherent limitations and difficulties. On the other hand, successful simulation results demonstrate the high potential of the hybrid approach.

© 2008 Published by Elsevier Ltd.

Contents

1. Introduction . . . 350
2. Basic concepts . . . 352
   2.1. Unsteady RANS . . . 352
   2.2. Large eddy simulation . . . 353
   2.3. Very large eddy simulation . . . 354
   2.4. Structural similarity of LES and RANS equations . . . 354
   2.5. Principal approaches to coupling LES with RANS . . . 355
3. Blending turbulence models . . . 356
   3.1. Damping of a RANS model (FSM) . . . 356
      3.1.1. Description of the method . . . 356
      3.1.2. The issue of consistency . . . 357
      3.1.3. Sample applications . . . 358
      3.1.4. Assessment and recommendations . . . 358
   3.2. A weighted sum of LES and RANS model . . . 359
      3.2.1. Description of the method . . . 359
      3.2.2. Sample applications . . . 359
      3.2.3. Assessment . . . 359
4. Interfacing RANS and LES models . . . 359
   4.1. Detached eddy simulation (DES) . . . 359
      4.1.1. Description of the method . . . 359
      4.1.2. Applications to flows with detached eddies . . . 360
      4.1.3. DES as a wall model . . . 360
      4.1.4. Enhancements of the basic method . . . 360
      4.1.5. DES and DDES for the flow over periodic hills . . . 361
      4.1.6. Assessment . . . 361

* Corresponding author. Tel.: +49 351 463 37607.
E-mail addresses: jochen.froehlich@tu-dresden.de (J. Fröhlich), vonterzi@its.uni-karlsruhe.de (D. von Terzi).
[1] Current address: Institut für Thermische Strömungsmaschinen, Universität Karlsruhe (TH), Kaiserstr. 12, 76131 Karlsruhe, Germany. Tel.: +49 721 608 6829.

0376-0421/$ - see front matter © 2008 Published by Elsevier Ltd.
doi:10.1016/j.paerosci.2008.05.001

4.2. Layering RANS and LES . . . 362
4.2.1. Definition of the interface location . . . 362
4.2.2. Description of methods . . . 363
4.2.3. Application to the flow over periodic hills . . . 364
4.2.4. Assessment and comparison with other near-wall treatments . . . 364
4.3. RANS-limited LES . . . 365
4.3.1. Description of the method . . . 365
4.3.2. Sample applications . . . 365
4.3.3. Assessment . . . 366
4.4. Limited numerical scales (LNS) . . . 366
5. Segregated modeling . . . 366
5.1. Inflow coupling . . . 367
5.2. Outflow coupling . . . 367
5.2.1. Enrichment . . . 368
5.2.2. Using a controller in an overlap zone . . . 368
5.2.3. Convective velocity coupling . . . 369
5.2.4. Sample applications . . . 369
5.3. Tangential coupling . . . 370
5.4. Assessment . . . 370
6. Second generation URANS models . . . 370
6.1. The PANS model . . . 370
6.1.1. Description of the method . . . 370
6.1.2. Sample applications . . . 370
6.1.3. Assessment . . . 370
6.2. Scale-adaptive simulation (SAS) . . . 371
6.2.1. Description of the method . . . 371
6.2.2. Sample applications and assessment . . . 372
6.3. Layering 2G-URANS and LES . . . 373
6.3.1. Description of the method . . . 373
6.3.2. First applications . . . 374
6.3.3. Assessment . . . 374
7. Concluding remarks . . . 374
Acknowledgements . . . 375
References . . . 375

1. Introduction

Each simulation of a turbulent flow is performed for a particular purpose. The minimum goal presumably is to determine the mean flow with acceptable precision. Further levels are the computation of higher moments or the determination of instantaneous unsteady features. Reynolds-averaged Navier–Stokes (RANS) models provide results for mean quantities with engineering accuracy at moderate cost for a wide range of flows [1]. In other situations, dominated by large-scale anisotropic vortical structures like wakes of bluff bodies, the average quantities are often less satisfactory when a RANS model is employed (see the ERCOFTAC/IAHR workshops on refined turbulence modeling [2–5], for example). Then large eddy simulation (LES) performs generally better and bears less modeling uncertainties. Furthermore, LES by construction provides unsteady data that are indispensable in many cases: determination of unsteady forces, fluid–structure coupling, identification of aerodynamic sources of sound, and phase-resolved multiphase flow, to name but a few issues. Unfortunately, LES is by a factor of 10 to 100 more costly than RANS computations [6]: LES requires a finer grid, cannot benefit from symmetries of the flow in space, and provides mean values only by averaging the unsteady flow field computed with small time step over a long sampling time. Hence, it seems natural to attempt a combination of both turbulence modeling approaches and to perform LES only where it is needed while using RANS in regions where it is reliable and efficient.

An illustration of this line of thought is given by the simulation of the flow around the so-called Ahmed body in Fig. 1 used in several of the above benchmarking activities [4,5]. The Reynolds number in the experiment was $Re = 7.68 \times 10^5$ based on the height of the body. This is a high value for *Re*, as it yields very thin attached boundary layers along the walls in the front part. Separation is induced by the corners at the rear. Up to an angle of about 30° of the slant, reattachment occurs at some position on the slant substantially increasing the drag [8,9]. The flow at and behind the trailing edge of the body is hence very complex and cannot reliably be simulated using RANS methods [5]. For this case, a viable hybrid LES/RANS strategy would consist of a so-called *embedded LES*, i.e. an LES zone in an otherwise statistical model in order to resolve the critical part of the flow.

Another and somewhat different motivation for LES/RANS coupling stems from wall-bounded flows. Close to walls, the LES philosophy of resolving the locally most energetic vortical structures requires to substantially reduce the step size of the grid since the dominating structures become very small in this region. Furthermore, when increasing the Reynolds number, the scaling of the computational effort is similar to that of a DNS in its dependence on *Re* just with a smaller constant [10]. That makes the approach unfeasible for wall-bounded flows at high *Re*, such as the flow over a wing [11]. As a remedy, some sort of wall model can be introduced to bridge the near-wall part of the boundary layer and to make the scaling of the required number of grid points independent of *Re*.

Near-wall models in the form of wall functions relying on the logarithmic law of the wall have been used since the very first LES [12,13]. Slightly rephrased, statistical information is used in place of higher resolution. Since then, this approach has been extended in different directions. Other scalings and wall laws can be used [14–16] as well as boundary layer equations in the wall-adjacent cell [17,18]. Details are given in reviews on LES, such as [19–21]. In this perspective it is natural to enhance the approach by

Nomenclature

Abbreviations

ADM	approximate deconvolution model
DDES	delayed DES
DES	detached eddy simulation
DNS	direct numerical simulation
FSM	flow simulation methodology
IC	initial condition
ILES	implicit LES
LES	large eddy simulation
LNS	limited numerical scales
MILES	monotonic integrated LES
MSD	modeled stress depletion
PANS	partially averaged Navier–Stokes
PDE	partial differential equation
POD	proper orthogonal decomposition
RANS	Reynolds-averaged Navier–Stokes
RNG	renormalization group
SAS	scale-adaptive simulation
SGS	subgrid scale
SST	shear–stress transport
URANS	unsteady RANS
VLES	very large eddy simulation
WALE	wall-adapted local eddy Viscosity
2G-URANS	second-generation URANS
2D, 3D	two-, three-dimensional
r.h.s.	right-hand side
w.r.t.	with respect to

Upper-case Roman

C	constant
C_p	pressure coefficient
E	spectral energy
F	model function in SAS
G, G_{Δ_f}	filter kernel
K	turbulent kinetic energy
K_τ	SGS kinetic energy
L, $L_{\mathrm{v}K}$	model length-scale in SAS
Ma	Mach number
P_K	turbulence production
$Q=(\Omega^2-S^2)/2$	vortex identification criterion
Re, Re_D, Re_τ	Reynolds number
R_{ij}	two-point correlation
S	strain-rate magnitude
St	Strouhal number
U_i, U	mean velocity (component)
U_b	bulk velocity
X_r	reattachment length

Lower-case Roman

c	constant
d	wall distance, coefficient in vortex method
f	arbitrary function
h	hill height
j	number of grid-line
k	wavenumber
ℓ	turbulent length-scale
n	model constant in FSM
p	pressure
r	distance, radius
t	time
u_i, u, v, w	velocity components
u_τ	friction velocity ($\sqrt{\langle\tau_\mathrm{wall}\rangle/\rho}$)
x_i, x, y, z	Cartesian coordinates
y^*	interface location

Upper-case Greek

Δ	model length-scale
Δ_f	filter width
Δ_g	characteristic step size of grid
Δ_x, Δ_y, Δ_z	step size of grid in x, y, z
Δ_t	time step
Φ	$\sqrt{K}L$
Ω	vorticity magnitude

Lower-case Greek

α	angle, latency factor in LNS
β, β^*	model coefficients
δ	characteristic length-scale
ε	turbulent dissipation rate
ε_τ	SGS dissipation rate
η	model coefficient
κ	von Kármán constant
λ	wavelength
ν	molecular viscosity
ν_t	eddy viscosity
$\tilde{\nu}$	modified eddy viscosity
ϕ	arbitrary variable
ρ	density
σ	model coefficient
τ, τ_{ij}	unresolved turbulent stresses
τ_wall	wall shear-stress
ω	$\varepsilon/(K\beta^*)$
ζ	model coefficient

Symbols and indices

$\langle\phi\rangle$	Reynolds average
$\tilde{\phi}$	phase average, modified quantity
ϕ'	fluctuation, first derivative
ϕ''	fluctuation, second derivative
$\overline{\phi}$	filtered quantity
$G*\phi$	convolution of G with ϕ
ϕ^+	near-wall scaling
ϕ_i, ϕ_{ij}	vector, tensor components
ϕ_{int}	value of ϕ at interface
∂_ϕ	derivative w.r.t ϕ
$\max\{\phi_1;\phi_2;\ldots\}$	maximum of ϕ_1, ϕ_2, etc.
$\min\{\phi_1;\phi_2;\ldots\}$	minimum of ϕ_1, ϕ_2, etc.

considering a full RANS model in the near-wall region and to combine it with an LES for computation of the outer flow. This is a second and slightly different attitude toward LES/RANS coupling. It constitutes the present high-complexity end of a fairly continuous scale of wall models for LES of increasing sophistication. Here, wall functions are not discussed, although they could also be viewed as a sort of LES/RANS coupling. Instead only near-wall models are considered that employ a full RANS transport equation discretized on a three-dimensional grid in the vicinity of the wall.

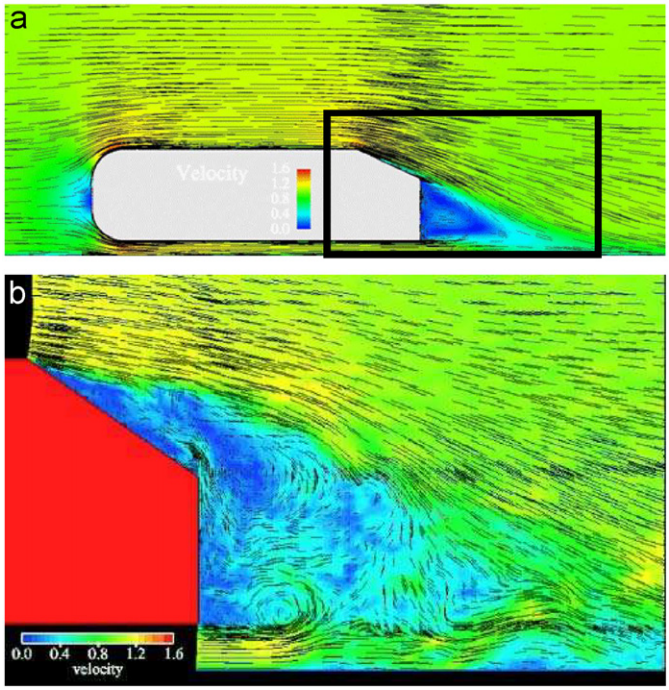

Fig. 1. LES prediction of the complete flow field over a simplified car geometry (Ahmed body) [7]: The boxed area in the top plot indicates the problematic region for RANS (see instantaneous flow below) on which an embedded LES would focus. (a) Mean flow; (b) instantaneous flow.

For ease of presentation, the pressure variable p is defined as the pressure divided by the density for the constant-density flows considered in the following. In Section 2, the basic concepts and underlying ideas with respect to (w.r.t.) the methodology of hybrid LES/RANS are recalled and a classification of the different methods is introduced. This classification is new and original work exceeding other attempts in the literature w.r.t. consistency and completeness. Discussions of individual methods are grouped according to this classification. First *unified models* are presented. These are distinguished between *blended models* and *interfaced models*. A certain number of the former type is discussed in Section 3. Interfaced models are described in Section 4. An altogether different approach to hybrid LES/RANS is *segregated modeling* (Section 5). Some methods, referred to as hybrid methods in the literature, do not fit into either category, since they are in fact *second generation URANS models* (2G-URANS) as explained below (URANS = unsteady RANS). These are discussed separately in Section 6. Beyond a mere description, a tentative assessment of the models is provided based on the information available so far. It constitutes the authors' current point of view, but the subject is still young and for some models only limited information is available.

2. Basic concepts

2.1. Unsteady RANS

Models employing the RANS equations are based on a definition of a mean, denoted $\langle\cdots\rangle$, which must have certain properties, such as $\langle\langle\phi\rangle\rangle = \langle\phi\rangle$ for any quantity ϕ [22,23]. Fluctuations w.r.t. the Reynolds-average are denoted by a prime. The averaging operation is applied to the Navier–Stokes equations yielding equations governing the mean motion of the flow. These equations contain an unclosed term which is replaced by the RANS model $\tau_{ij}^{\mathrm{RANS}}$. Typically, the model coefficients are calibrated by means of prototypical flows which are desired to be captured [24].

There exist several ways to define the operator $\langle\ldots\rangle$. The conceptually soundest is the mathematical expectation, but other definitions can be used for flows with certain properties [23]. For statistically steady flows, the temporal mean is an appropriate choice. For flows with slow variation of statistical properties (slow compared to the characteristic turbulent time-scale) a finite-time temporal average can be used [24]. For unsteady flows with some basic frequency, a phase average can be introduced. In this latter case a triple decomposition

$$u_i = \langle u_i\rangle + \tilde{u}_i + u_i' \tag{1}$$

for the velocity vector u_i was proposed in [25] with $\tilde{u}_i$ being the phase average or the average conditioned on some slowly varying quantity. It has become common to name RANS modeling as URANS whenever the computed solution is time-dependent. The approach then is to apply an existing RANS model and to aim at resolving some of the unsteady features of the flow without recalibration of model coefficients.

With respect to large-scale unsteadiness (large in space and time, as opposed to turbulent fluctuations) it is useful to distinguish between two cases. In many situations the boundary conditions are unsteady, for example, when the mass flux through an inlet with turbulent flow conditions changes in time. Such variation generally is substantially slower than the turbulent time-scales and, hence, any direct interaction can be neglected. This constitutes a situation with scale separation. The modeling assumptions for the RANS models are then valid and, most of all, unsteadiness of statistical mean values is triggered from the exterior.

A second case, comprises situations with internal instabilities of the flow, such as bluff body flows. In the near field, scale separation usually does not hold: The very largest vortical structures depend on details of the transition process (influenced by the thickness of some boundary or shear layer, etc.) and disintegrate into smaller and smaller structures farther downstream. In such a situation, phase averages can be constructed and the terms in the RANS equations can be properly defined. However, a substantial amount of interaction between turbulent fluctuations unresolved by the URANS approach and the resolved fluctuations occurs which is delicate to handle. It is the second step, devising a model for this situation, which poses the problem. An unmodified RANS model is likely to be unsuitable for this task.

A good illustration of these arguments is provided by the flow around a square cylinder investigated in [26], where URANS with a Reynolds stress model and a K–ε model were performed as well as full LES. An excerpt of these results is shown in Fig. 2. The grid was three-dimensional in both cases with a factor of about ten in the total number of grid points employed. This complies with the URANS philosophy of resolving only the very largest motions, hence allowing for a coarser grid compared to LES. The URANS solution which developed in the simulation is seen to be mostly two-dimensional. In fact, some URANS computations employ a two-dimensional discretization right from the start. The URANS results considered here do not yield the correct Strouhal number St. This frequency, however, is a very insensitive quantity for most bluff body flows.[1] Hence, if not even St is correctly captured, no confidence in the results can be attested at all. If, on the other hand, St matches the experimental value, this does not suffice to demonstrate that the simulation as successful [27].

[1] In a lecture at the Von Kármán Institute, J. Ferziger coined the phrase: "You throw dice and you get the Strouhal number."

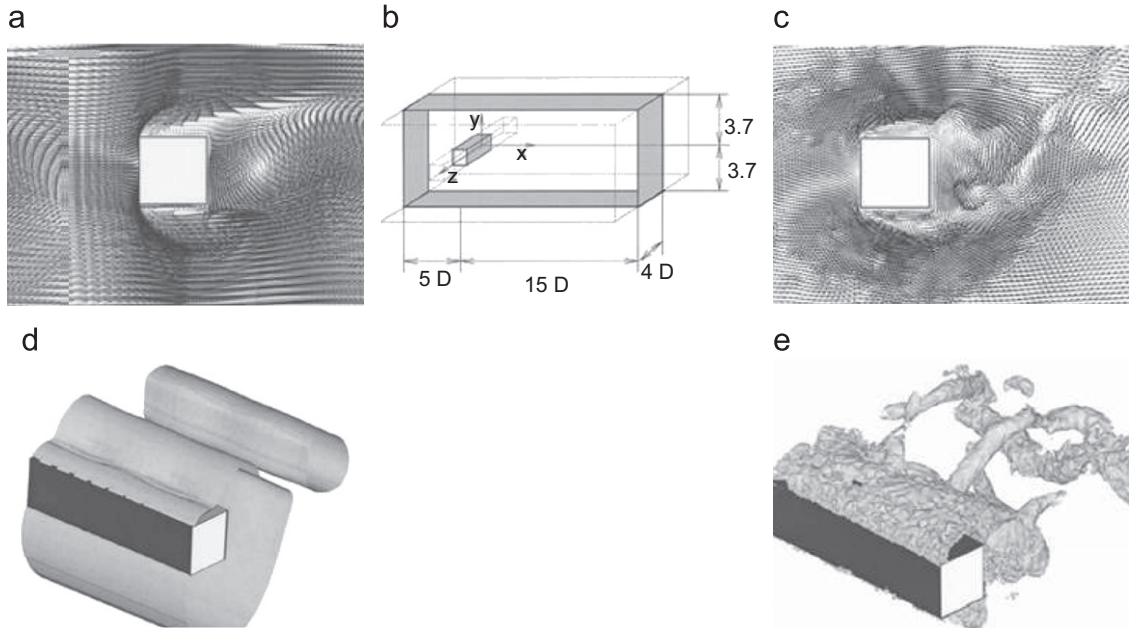

Fig. 2. Simulations of the flow over a square cylinder: instantaneous velocity and pressure fields for URANS (left, $St = 0.121$) and LES (right, $St = 0.144$); experiments (not shown, $St = 0.143$); $Re_D = 10^5$ [26]. (a) URANS: velocity; (b) geometric setup; (c) LES: velocity; (d) URANS: pressure; (e) LES: pressure.

The example given here illustrates the difficulties traditional URANS calculations may encounter. On the other hand, URANS simulations can be substantially more successful in determining the mean flow than a steady RANS computation [28]. In our opinion, the main concern when applying URANS is the confidence one can have in the results when no experimental data are available for validation. Sometimes grid convergence is not achieved in the range of commonly employed grid resolutions [29]. The use of URANS can hence only be advocated in cases of clear scale separation as described in the beginning of this section. When this is not the case, as in the second situation discussed, the approach seems delicate.

2.2. Large eddy simulation

LES is often introduced based on the filtering concept [30]. If a spatial filter $G = G_{\Delta_f}$ is applied to a variable ϕ this yields a smoothed counterpart $\overline{\phi}$ with scales smaller than the filter width Δ_f being removed. Although technically difficult near walls and other complex situations, this filter is considered to be some sort of convolution, i.e. $\overline{\phi} = G * \phi$, with generally $\overline{\overline{\phi}} \neq \overline{\phi}$. As for RANS modeling, the nonlinear convection term in the transport equation introduces an unclosed term, describing the impact of the subfilter scales on the resolved motion, it is replaced by a model term τ_{ij}^{LES}. The filter width Δ_f then has to appear as a parameter in the model, usually called Δ. Note, however, that in most LES, filtering is rather a concept behind the development of the method than an explicitly applied procedure to specify the resolved motion [31].

For efficiency reasons the ratio of the filter width Δ_f to the step size of the grid Δ_g is usually set equal to one or to a small integer. The step size of the grid hence determines the cutoff scale of the filter and therefore the corresponding parameter in the model. For these and also for historical reasons, τ_{ij}^{LES} is usually called subgrid-scale (SGS) model. The aim with $\Delta \sim \Delta_g$ is to benefit to a maximum from the resolution capacity of the grid in shifting the cutoff of the implicitly introduced filter to higher wavenumbers if the grid is refined. Hence, in the ultimate limit

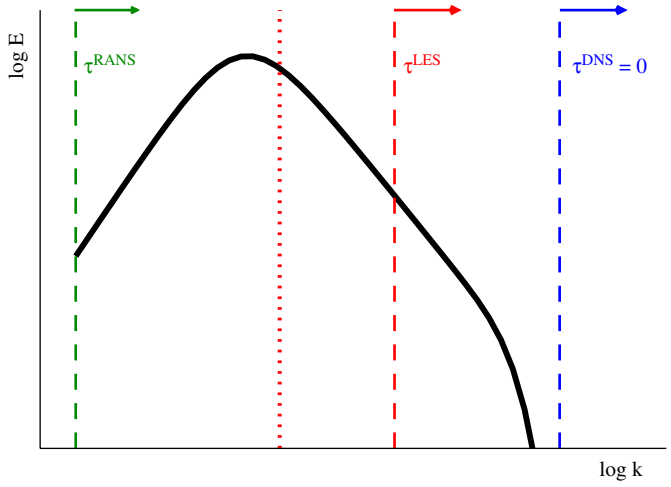

Fig. 3. Idealized spectrum of turbulent kinetic energy of isotropic turbulence with respect to the wavenumber k and schematic of the extent of modeling employed by the traditional simulation strategies DNS, LES, and RANS. The vertical dotted line marks the aim of VLES and corresponding hybrid LES/RANS methods.

$\Delta_g \to 0$, the SGS model vanishes so that the simulation turns into a direct numerical simulation (DNS) without turbulence model (see Fig. 3).

The basic strategy with LES is to resolve most of the turbulent kinetic energy K of the flow, while modeling most of the dissipation ε. The possibility of this separation arises from the fact that K is determined by the large scales of motion and ε by the small scales [32]. The promise of LES is that simple models will suffice since the modeled components are remote in scale from the resolved ones [33]. As a rule of thumb, K should be resolved to at least 80% to warrant reliable results [23]. The concept, although clear and simple, works well for high-Reynolds number flows remote from boundaries but bears practical difficulties for high-Re flows near walls, for transitional flows and for the specification of inflow data.

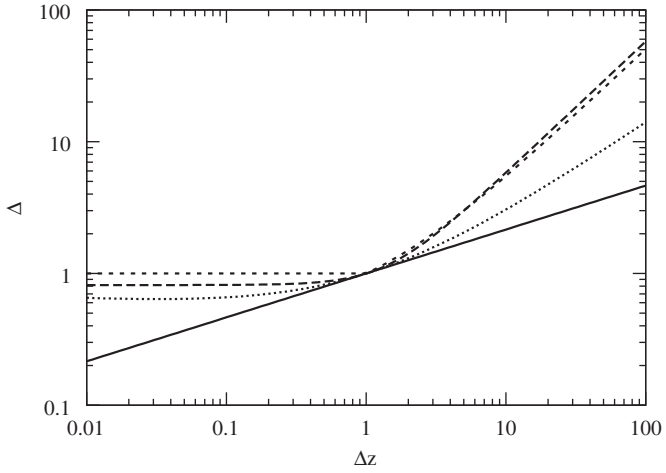

Fig. 4. Grid scale Δ_g determined according to the three equations given in the text: (2) (——), (3) (– – –), (4) (- - - -), reproduced from [21]. In the figure, the value from (3) was divided by $\sqrt{3}$. The fourth relation (· · ·) was proposed by Scotti [35]. To achieve a coherent picture only Δ_z is varied, whereas Δ_x and Δ_y were set to one. For $\Delta_z<1$ flat cells are obtained, for $\Delta_z>1$ the cells have the shape of needles.

Another question repeatedly discussed in the literature on hybrid LES/RANS methods is the choice of an expression for $\Delta\sim\Delta_g$ in the case of strongly anisotropic grids (the index g will be dropped from now on). The issue principally is an LES-issue but it is relevant in the present context, particularly when considering near-wall flows where typically anisotropic grids are employed. Many hybrid methods rely on Δ not only as part of the LES model but also when interfaces or blendings between LES and RANS are determined.

The expression most often used for LES is the geometric mean

$$\Delta_g = (\Delta_x\ \Delta_y\ \Delta_z)^{1/3} \tag{2}$$

or its generalization, the cubic root of the cell volume. In case of anisotropic grids, definition (2) tends to provide a fairly low value, as illustrated in Fig. 4. For this reason, the quadratic mean

$$\Delta_g = \left(\frac{\Delta_x^2+\Delta_y^2+\Delta_z^2}{3}\right)^{1/2} \tag{3}$$

is advocated in some publications. Other authors favor the maximum [34]

$$\Delta_g = \max\{\Delta_x;\Delta_y;\Delta_z\}. \tag{4}$$

2.3. Very large eddy simulation

Based on the initial successes of LES in predicting prototypical flows, attempts have been made to apply traditional LES to complex flows of industrial relevance. With the computer resources available, however, the resulting computational grids necessarily had to be coarse—too coarse to resolve the desired amount of kinetic energy, and therefore were called very large eddy simulation (VLES) by some researchers [36]. This approach (even with adjusting model constants) did not meet with success. First, the LES cutoff is now located within or even below the wavenumber range of the most energetic modes. Modeling the interaction between the resolved motion and the unresolved motion is very delicate in this case, and there is little hope for success. Second, the numerical discretization scheme, mostly disregarded in the classical LES model development, impacts on the scales near the grid scale which are the physically relevant ones with VLES.

An illustration of the first point addressed here can be given using a typical spectrum of turbulent flow displayed in Fig. 3. A traditional SGS model, e.g. the Smagorinsky model, and a grid sufficiently fine to resolve the inertial range of the turbulent spectrum will yield excellent results, since this is a scenario for which such a model is designed and calibrated. For this case, the length scale Δ used in the SGS model is much smaller than the scales of turbulence containing most of the energy as reflected by the maximum in Fig. 3. These scales are characterized by the integral length-scale $\ell = K^{3/2}/\varepsilon$. Production of turbulent fluctuations occurs at these larger scales which are well resolved. The unresolved dissipation is related to Δ by the SGS model. Increasing the step size of the grid increases Δ and the dissipation of the model. As a consequence, the impact of the model on the resolved flow field increases. Once large amounts of kinetic energy are unresolved, i.e. latest when the grid spacing is of the order of ℓ, the LES results start to deteriorate. Then turbulence production is not resolved anymore whereas dissipation is largely overpredicted. Traditional SGS models contain no mechanism that stops them from increasing the turbulent dissipation beyond physical meaningful values.

Despite the failure of the naive approach, the idea to predict the large-scale unsteadiness of the flow at minimum cost remains attractive and such coherent structure capturing, as it was called by Ferziger [36], is the aim of many hybrid LES/RANS methods. This however requires a substantially more sophisticated modeling approach. In the literature, the acronym VLES has occasionally been used synonymously for a wide range of methods [37] such that this term is not descriptive anymore. Here, we will restrict VLES to its original intent: LES performed with traditional SGS models on coarse grids. VLES in this sense cannot be recommended. A rare exception is the generation of inflow conditions for LES [38,39].

2.4. Structural similarity of LES and RANS equations

For the sequel it is necessary to define the specifics of LES models and RANS models. Using an unsteady definition of a Reynolds average as discussed above, the transport equations for the Reynolds-averaged velocity $\langle u_i\rangle$ read

$$\partial_t\langle u_i\rangle + \partial_{x_j}(\langle u_i\rangle\langle u_j\rangle) + \partial_{x_i}\langle p\rangle = \partial_{x_j}(\nu\partial_{x_j}\langle u_i\rangle) - \partial_{x_j}\tau_{ij}^{\mathrm{RANS}}. \tag{5}$$

The analogous equations for the resolved velocity $\overline{u}_i$ in an LES read

$$\partial_t\overline{u}_i + \partial_{x_j}(\overline{u}_i\overline{u}_j) + \partial_{x_i}\overline{p} = \partial_{x_j}(\nu\partial_{x_j}\overline{u}_i) - \partial_{x_j}\tau_{ij}^{\mathrm{LES}} \tag{6}$$

(recall that p is the density-divided pressure). The obvious similarity is further enhanced by the usage of the eddy viscosity concept for most SGS and the fact that the employed models are often derived from RANS counterparts. As a consequence, not only the governing equations exhibit a structural similarity, but also many of the turbulence models.

A RANS model depends on physical quantities describing the entirety of the turbulent fluctuations. For example, the K–ε model determines

$$\tau_{ij}^{\mathrm{RANS}} = f(\partial_{x_i}\langle u_i\rangle, K, \varepsilon, C), \tag{7}$$

where C is a model constant, K the turbulent kinetic energy, and ε the turbulent dissipation rate. The latter two are determined from other relations, but this is of no matter here. LES based on the Smagorinsky model uses a relation like

$$\tau_{ij}^{\mathrm{LES}} = f(\partial_{x_j}\overline{u}_i, \Delta, C), \tag{8}$$

where Δ is a length scale related to the numerical grid, e.g. $\Delta = (\Delta_x \Delta_y \Delta_z)^{1/3}$. Since there exist many variants of LES and RANS models we define the following: a model qualifies as an LES model if it explicitly involves in one or the other way the step size of the computational grid. RANS models, in contrast, only depend on physical quantities, including geometric features like the wall distance.

Mathematically a partial differential equation problem is well-posed only if appropriate initial and boundary conditions are specified together with the equation. For turbulent flows with stationary statistics, initial conditions (ICs) are a minor issue, since they are generally "forgotten" after a short time. Boundary conditions, on the other hand, are often more important and it is seen below in the context of DES, for example, that a RANS model conceived for computing a steady solution can be forced to run in an unsteady mode by supplying it with unsteady boundary conditions.

Another concept is also important here, the concept of implicit filtering [40]. Suppose, the LES model in (6) were exact. Then, the computed quantity, here denoted $\overline{u}_i$, would exactly equal $G * u_i$. Hence, changing the point of view it can be said that the exact model term, by means of the evolution of the transport equations, determines the filter G. Further on this line of thought we may say that the applied model term determines the quantity being computed. Forgetting about the different notation of the unknowns in (5) and (6), it is the fact that τ_{ij}^{LES} or $\tau_{ij}^{\mathrm{RANS}}$ is used in the equation which determines whether the computed solution is a RANS solution or an LES solution.

Based on the implicit filtering idea, there are approaches, where Δ in an SGS model and hence the implicit filter is not related to the numerical grid but directly specified as an independent length scale by the user [40,41]. Extending the above definition to include these situations, we call LES a method where the user specifies the meaning of "large" by providing a length scale, be it directly or via the grid. This definition also covers LES with explicit filtering techniques, like approximate deconvolution model (ADM) [42] or high-pass filtered eddy viscosity models [43], and implicit SGS models such as monotonic integrated LES (MILES) [44], implicit LES (ILES) [45], etc. For these methods either the filter width is prescribed or the truncation error of the numerical scheme serves as the SGS model with the strongest attenuation of fluctuations occurring at wavenumbers related to the grid-size. On the other hand this generalized definition of LES does not cover methods where a certain fraction of the turbulent kinetic energy is required to be resolved as discussed below, since that specifies the energy contents and not a length scale.

2.5. Principal approaches to coupling LES with RANS

The similarity of the equations and the considerations in Section 2.4 suggest the concept of *unified modeling*. This approach is based on using the same transport equation for some resolved velocity $\overline{u}_i$, yet to be specified in its meaning:

$$\partial_t \overline{u}_i + \partial_{x_j}(\overline{u}_i \overline{u}_j) + \partial_{x_i} \overline{p} = \nu \partial_{x_j} \partial_{x_j} \overline{u}_i + \partial_{x_j} \tau_{ij}^{\mathrm{model}}, \tag{9}$$

or, if an eddy viscosity ansatz is used,

$$\partial_t \overline{u}_i + \partial_{x_j}(\overline{u}_i \overline{u}_j) + \partial_{x_i} \overline{p} = \partial_{x_j}\left((\nu + \nu_t)\partial_{x_j} \overline{u}_i\right). \tag{10}$$

A transition from LES to RANS can be achieved in several ways. One possibility is *blending*, i.e. by a weighted sum of a RANS model and an LES the models according to

$$\tau_{ij}^{\mathrm{model}} = f^{\mathrm{RANS}} \tau_{ij}^{\mathrm{RANS}} + f^{\mathrm{LES}} \tau_{ij}^{\mathrm{LES}}. \tag{11}$$

In this equation f^{RANS} and f^{LES} are local blending coefficients determined by the local value of a given criterion.

Another strategy is to use a pure LES model in one part of the domain and a pure RANS model in the remainder, so that a boundary between a RANS zone and an LES zone can be specified at each instant in time. The transport equation for the velocity, however, is the same in both zones with no particular adjustment other than switching the model term at the interface. This way the computed resolved velocity is continuous. We term this strategy *interfacing LES and RANS*. Furthermore, if the interface is constant in time, it is called a *hard interface*. If it changes in time depending on the computed solution, it is termed a *soft interface*.

Unified modeling is simplified by the fact that many LES models are inspired from RANS models and hence bear the same structure. The eddy viscosity concept used for illustration in (10) is one instance. Others are observed as well, such as the use of a transport equation for the turbulent kinetic energy of the unresolved motion. With RANS, this is an equation for the turbulent kinetic energy $K = \langle u_i' u_i' \rangle$, while with LES, this is an equation for the trace of the SGS tensor $K_\tau = \tau_{ii}/2$. This quantity is often called SGS kinetic energy. Further examples will be encountered below. In principle, any RANS model can be turned into an LES model according to the above definition by introducing the step size of the grid as a length-scale of the model, allowing to reduce the amount of damping of the resolved motion if the grid is refined. This approach leaves room to specify the particular way of blending or interfacing the models as illustrated by the examples in Sections 3 and 4, respectively.

Instead of switching the model, a hybrid method can also be constructed by employing everywhere the same secondary transport equations for a given model, may it be a RANS or an LES model, and merely adjust some terms in these equations. This modification should be designed to alter the model behavior from RANS to LES, or vice versa. Thereby it is commonly more practical to turn a state of the art RANS model into an acceptable SGS model for LES than the other way round. This could be achieved by switching at the interface to the step size of the grid as a model length-scale in selected terms of a transport equation.

Segregated modeling is the counterpart to unified modeling. LES is employed in one part of the computational domain, while RANS is used in the remainder. With segregated modeling, however, the resolved quantities are no more continuous at the interfaces. Instead, almost stand-alone LES and RANS computations are performed in their respective subdomains which are then coupled via appropriate boundary conditions. Except for laminar flows, the solution is discontinuous at these interfaces. This avoids any gradual transition in some gray area characteristic of unified turbulence models. Segregated modeling allows for *embedded LES* by designing a configuration where in an otherwise RANS simulation a specific region is selected to be treated with LES—with full two-way coupling between the zones (see Fig. 5).

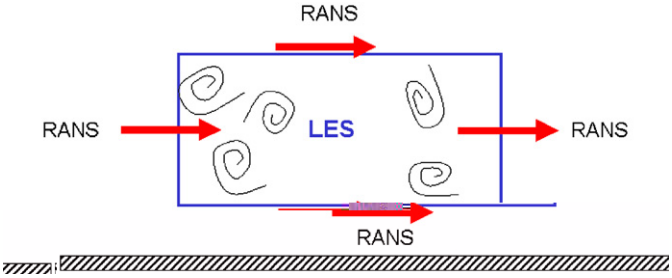

Fig. 5. Possible types of interfaces between an embedded LES and the surrounding RANS region, here illustrated with segregated modeling.

Let us mention that in the literature the terminology *zonal* (together with its counterpart *non-zonal*) is frequently used to classify hybrid LES/RANS methods in the sense that there exist well-defined LES zones and RANS zones. The precise meaning of the term zonal varies in different publications. It is straightforward to identify segregated modeling as a form of zonal coupling and some methods following the paradigm of unified modeling as non-zonal. In fact, in their recent review, Sagaut et al. [46] distinguish two main classes of hybrid LES/RANS methods: "zonal" or "global" models, which match the definitions of segregated and unified modeling, respectively. But there is also frequent ambiguity. For many hybrid methods it is possible to discern a RANS zone within the computational domain which is distinct from the region computed with LES—whether these zones change in course of a simulation or not. Some researchers then use the term "zonal" to identify only methods where the boundaries of these subdomains are constant in time. The distinction is hence made by the stationarity of the RANS and LES regions and only indirectly on how the hybrid method was devised. Others choose to distinguish zonal from non-zonal if the subdomains are predefined by the user. For example, the unified model with a stationary, user-defined border between the LES and RANS subdomains employed in [47], although categorized in [46] as a global model, was also given the attribute "zonal" in front of its name. Moreover, even for methods where the location of the interface between zones is determined by the solution itself, say a functional of the mean shear-stress at the closest wall, it also depends, often indirectly, on parameters and/or the grid specified by the user a priori. This is the reason why, with some justification, such methods might also be considered to employ user-defined coupling. Due to the ambiguities associated with the terms zonal and non-zonal the present terminology is preferred (see also Fig. 28).

Regardless how precisely the coupling between different regions with different models is accomplished, four principal situations can be distinguished. These are best illustrated with segregated modeling but carry over to all other hybrid methods. Fig. 5 shows a situation of an LES embedded in a RANS solution which is assumed to be steady. Taking the perspective of the LES domain, the left-most boundary is an LES-inflow boundary. The steady RANS solution however does not provide any turbulent fluctuations. Performing LES on the downstream side of the interface, on the other hand, requires proper LES-boundary conditions, i.e. realistic turbulent fluctuations. The problem hence is the same as with LES-inflow conditions discussed in reviews of LES and briefly detailed in Section 5.1. The second situation is the one of an LES-outflow boundary. At first sight it seems trivial since most LES are performed with a downstream outflow. Here, however, as a more general case, the interface must allow for information to be propagated upstream if the RANS simulation downstream of the LES zone is to be of any use at all [48].

The third situation is the one of tangential coupling. A distinction between two situations can be made: near-wall flow and coupling to an outer flow. With a RANS zone between the wall and the LES region, is not obvious whether the right amount of resolved fluctuations is obtained in the LES zone near the interface. This becomes clear if, for example, one assumes a naive gluing of LES and RANS by a continuous discretization of the velocity field and its equations of motion and switch the turbulence model at the interface, from ν_t^{RANS} to ν_t^{LES}. The LES solution is then damped near the interface by the steady or slowly evolving RANS solution and hence is likely to exhibit a fluctuation deficit. The RANS model on the other side of the interface receives fluctuations from the LES and is thus pushed toward an unsteady mode. This can lead to *double accounting* of fluctuations, once by the RANS model conceived to represent the entirety of fluctuations, and second by the resolved motion on the RANS side. Even more: increasing gradients of the resolved flow in the RANS region can increase ν_t^{RANS} beyond the steady RANS value via its dependence on the velocity gradients. On the other hand, for many applications the outer tangential boundary can be regarded as similar to the outflow boundary [49] and may hence be less critical.

3. Blending turbulence models

According to Speziale [50,51], a good unified turbulence model should possess at least three properties: (1) in the coarse grid limit, the hybrid should turn into a RANS model, (2) for well-resolved simulations a DNS should be recovered, and (3) no explicit filtering or averaging should be applied. The first property rules out traditional VLES as discussed in Section 2.3. The second necessitates an estimation of the local resolution such that the model can switch itself off. This introduces a dependency of the hybrid formulation on the step size of the grid. The last property was supposed to ease the application of the model to flows in complex geometries with highly stretched grids and no homogeneous directions and was an argument against the use of some of the advanced SGS models favored at the time.

Since hybrid LES/RANS are intended for complex flows where many simplified modeling assumptions are likely to be invalid, Speziale insists that a state-of-the-art RANS model should be recovered in case of coarse resolution. Such a model contains at the very least two auxiliary transport equations for independent scales used in the turbulence model and can account for some effects of anisotropy and curvature due to a nonlinear relation of turbulent stresses and the resolved strain-rate and vorticity tensors.

3.1. Damping of a RANS model (FSM)

Unified turbulence models fulfilling the above demands can be constructed by resolution-dependent damping of a RANS model [50,51]. This approach is neither classical RANS nor classical LES. It was therefore given the general name flow simulation methodology (FSM) by collaborators of Speziale [52,53].

3.1.1. Description of the method

The key idea of FSM is to determine the model term in (9) as

$$\tau_{ij}^{\mathrm{model}} = f_\Delta\left(\frac{\Delta}{\ell_K}\right)\tau_{ij}^{\mathrm{RANS}} \quad \text{with } 0 \leqslant f_\Delta \leqslant 1. \tag{12}$$

This decomposes the hybrid model into two factors: the RANS model and the so-called contribution function $f_\Delta(\Delta/\ell_K)$. The RANS model is responsible for the physical modeling of all turbulence and depends only on physical quantities. Any kind of RANS model can be used, but following the recommendations of Speziale, explicit algebraic Reynolds stress models with strain-rate dependent coefficients have mostly been applied. Using the K–ε or the K–ω model, on the other hand, yielded almost as good results in many applications [54].

The role of f_Δ is to damp the contribution of the RANS model, since part of the turbulence is resolved in an intermediate regime where the solution becomes unsteady. In fact, the issue is not the resolution of the kinetic energy but the resolution of the dissipation which, if not resolved, has to be provided by the model. If the grid is so fine that the entire dissipation range is resolved, the model should switch itself off. The idea hence is to estimate the "distance from DNS" by computing the factor Δ/ℓ_K,

where Δ represents the local grid size. Speziale suggested to use the Kolmogorov length-scale $\ell_K \approx \nu^{3/4}/\varepsilon^{1/4}$. Hence, the RANS model equations need to be solved not only to compute $\tau_{ij}^{\mathrm{RANS}}$, but also to obtain an estimate for ℓ_K.

The constraint $0 \leqslant f_\Delta \leqslant 1$ ensures that FSM can approach an URANS for coarse grids, coarse compared to ℓ_K, and a DNS for fine grids, i.e. a grid size of the order of ℓ_K. This is depicted in Fig. 6. FSM works fine in both limits, since the RANS model was conceived for this purpose and the DNS is free of any model. In between these two extremes, FSM can be classified as a kind of "untraditional" LES bridging the gap between LES and RANS. How well it performs in this regime depends on the contribution function, but also on whether the separation of variables assumed in (12) is valid or not, and last but not least on the grid and boundary conditions employed.

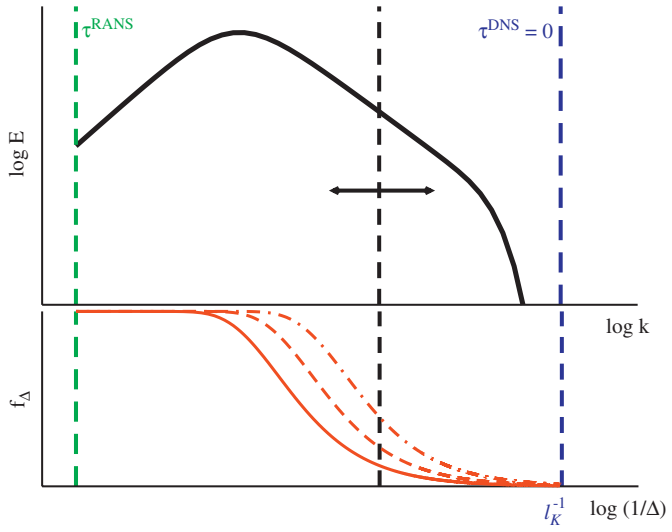

Fig. 6. Illustration of the FSM approach based on damping a RANS model by means of a damping function f_Δ. The solid black curve sketches the ideal energy spectrum with respect to wavenumber. The end of the dissipation range is marked by the Kolmogorov wavenumber proportional to ℓ_K^{-1}. The vertical dashed line in the center symbolizes the grid scale proportional to Δ^{-1}. The curves in the lower part of the figure illustrate the damping function of (13) for various values of β at fixed ℓ_K (and $n = 1$).

Fig. 7. Contours of the FSM damping function for the start-up vortex behind a backward-facing step; $Re = 3000$; red: high values, blue: low values.

In [51] the contribution function

$$f_\Delta\left(\frac{\Delta}{\ell_K}\right) = \left(1 - e^{-\beta\frac{\Delta}{\ell_K}}\right)^n, \tag{13}$$

was proposed on a phenomenological basis, using $\beta = 0.001$ and $n = 1$. The parameter n controls the steepness of the function and β determines at what resolution level the model contribution becomes negligible. The role of β was investigated in [52] where also a slightly different form of the contribution function was tested. Other versions of f_Δ were tested as well, e.g. a linear form, more applicable to the URANS limit or, in order to account for strongly anisotropic grids, different values of β for the scaling of different components of $\tau_{ij}^{\mathrm{RANS}}$ based on *a posteriori* analysis of DNS data. For the test cases studied, however, no particular improvements over the original form were observed.

Hussaini et al. [55] worked on deriving forms for f_Δ on a more rigorous basis, while still choosing parameters in an *ad hoc* fashion. An exponential form similar to (13) turned out to be a useful choice. On the other hand, Δ/ℓ_K was replaced by Δ^2, thus removing the estimate of the physical resolution. First results for the so-called Kolmogorov flow were promising. Another issue is the choice of Δ for strongly anisotropic grids typical for wall-bounded turbulent flows. Speziale [51] proposed to use the geometric mean (2), whereas for the examples given below, the quadratic mean (3) was employed.

In general, f_Δ varies in space and time, as is illustrated for the example of a startup vortex behind a backward-facing step in Fig. 7. It is this local and instantaneous damping of a RANS model that empowers FSM to compute as DNS, LES, and RANS at different locations in space and different instants in time within the same simulation. Since f_Δ involves the step size of the grid, FSM is an LES method according to the above definition.

3.1.2. *The issue of consistency*

FSM yields the resolved velocities $\overline{u}_i$. On the other hand, $\tau_{ij}^{\mathrm{RANS}}$ depends on the Reynolds-averaged velocity field $\langle u_i \rangle$ and two independent characteristic scales of the turbulence, say K and ε. A problem that is frequently overlooked is how to obtain $\langle u_i \rangle$, K and ε in a consistent fashion.

In the RANS limit of FSM, $\tau_{ij}^{\mathrm{model}} = \tau_{ij}^{\mathrm{RANS}}$ and solving the governing equations yields the velocity field $\overline{u}_i \equiv \langle u_i \rangle$ consistent with the Reynolds-averaging operations and hence the assumptions in deriving the Reynolds stress model. This velocity field is the required input when determining $\tau_{ij}^{\mathrm{RANS}}$ and also for solving the K–ε equations. On the other hand, beyond the RANS limit, necessarily $\tau_{ij}^{\mathrm{model}} \neq \tau_{ij}^{\mathrm{RANS}}$ so that $\overline{u}_i \neq \langle u_i \rangle$. Hence, one should determine $\langle u_i \rangle$ and use it in the RANS model. An explicit averaging operation in one homogeneous direction $\langle \overline{u}_i \rangle$ was performed in the first example below. Note that employing a two-dimensional time-dependent Reynolds-averaged flow field $\langle \overline{u}_i \rangle(t)$ and hence two-dimensional time-dependent contribution function and

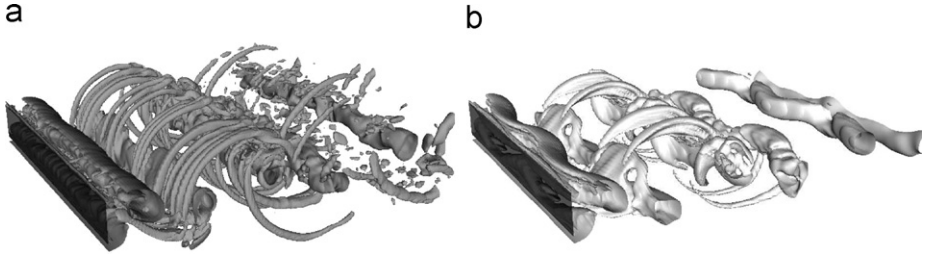

Fig. 8. Comparison of DNS and FSM for the flow over a bluff body: contours of $Q = (\Omega^2 - S^2)/2 = 1$; $Re = 1000$; $\beta = 4 \times 10^{-3}$; $n = 1$. Figures reproduced from from [54]. (a) DNS (eight million cells); (b) FSM (one million cells).

Reynolds stresses does not imply that the resulting flow field $\overline{u}_i$ has to be two-dimensional. The resolved flow field can be unstable w.r.t. three-dimensional perturbations and develop corresponding fluctuations as observed in Fig. 8. On the other hand, it was tried to skip the additional Reynolds averaging and directly use $\overline{u}_i$ instead of $\langle u_i \rangle$. This can work well as illustrated by the second example below and yields a fairly robust and inexpensive method [54].

3.1.3. Sample applications

The first example, shown in Fig. 8, is the flow over a square bluff body at $Re = 1000$. A DNS was performed using roughly eight million cells in physical space (a Fourier method was used in the spanwise direction). The dominant vortex shedding frequency was $St = 0.21$. The FSM was computed with only one million cells using $\beta = 4 \times 10^{-3}$ and $n = 1$. The RANS-model transport equations for K and ε were solved in two dimensions only using the spanwise averaged resolved velocities. In contrast to the URANS results for the square cylinder flow in Section 2.1, the same Strouhal number as in the DNS was obtained and the computed solution was three-dimensional. Using a vortex identification criterion the same kind of Kelvin–Helmholtz type vortices with deformations in the spanwise direction as in the DNS can be seen. Of course, less small-scale structures are observed since they cannot be resolved on the coarser grid.

Another example of a successful FSM application is the computation of the flow over an axisymmetric body with a blunt base at supersonic speeds ($Ma = 2.46$) and $Re = 3.3 \times 10^6$. This Reynolds number is too high for DNS or even traditional LES, whereas RANS simulations are not able to predict the base drag correctly. In [56] the flow was computed with a compressible extension of FSM [57,54] employing roughly two million grid points. Contrary to the example above, the transport equations for K and ε were solved on the three-dimensional grid using the resolved velocities directly. In addition, $f_\Delta = 1$ was enforced in the supersonic approach flow upstream of the base forcing the thin boundary layer to be computed in RANS mode. The separated flow becomes unsteady and the dominant flow structures are revealed in Fig. 9a using the vorticity magnitude. Detailed comparisons of FSM results with DNS data for lower Reynolds numbers can be found in [54,58]. The base-pressure coefficient presented in Fig. 9b is a central quantity to be predicted. A state-of-the-art RANS solution exhibits an unphysical pressure peak at the axis, while the FSM result matches the experimental values. This is still the case if the grid is altered or if β is varied [56]. In the latter reference, DES (see Section 4.1) was also performed on the same grid, but using a different flow solver with a lower order numerical method. The results were substantially worse, but improved for finer resolution [59]. Applications of FSM for parameter studies w.r.t. flow control for the baseflow can be found in [60].

3.1.4. Assessment and recommendations

Resolution-damped RANS models use the same turbulence model in the entire computational domain and base the model contributions on the actual resolution, thus producing a smooth transition. By design, they are consistent with RANS for coarse grids while retaining an eddy-resolving capability for a sufficiently well-resolved simulation. As a result, they are user-friendly since the transition between RANS and LES occurs in the equations without user-interference. However, all difficulties are now shifted to choosing the "appropriate grid," which is not a trivial task.

FSM has been applied for some years now and several successes have been reported. The method works particularly well for flows with strong instabilities, e.g. featuring geometries with sharp corners and separated flows. Problems may arise if information on unsteady structures of a region in RANS mode is crucial to the outcome of the simulation and, therefore, needs to be generated in a region of higher resolution. This is illustrated in Fig. 10. Suppose that at an upstream location the grid scale can be represented by the left vertical dashed line leading to the corresponding spectrum of the resolved motion. When the turbulent flow is transported by the mean flow into a region of higher resolution the high-wavenumber content is not yet existing and needs to be produced by the turbulence cascade or by flow instabilities (see also the discussion in [61]). This problem can be tackled by two approaches: (1) Treat an upstream RANS region as an LES-inflow situation and use a standard technique to generate appropriate fluctuations, such as synthetic turbulence, stochastic forcing, etc. (2) Resolve the physics if they are that

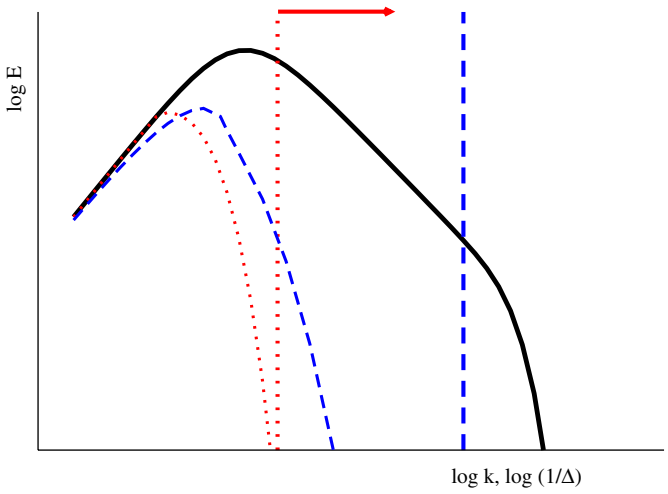

Fig. 10. Effect of sudden grid refinement on the resolved motion of turbulence: ideal spectrum of kinetic energy (solid line) and predicted spectrum before (dotted) and shortly after (dashed) the increase in resolution; vertical lines indicate the corresponding grid scale Δ.

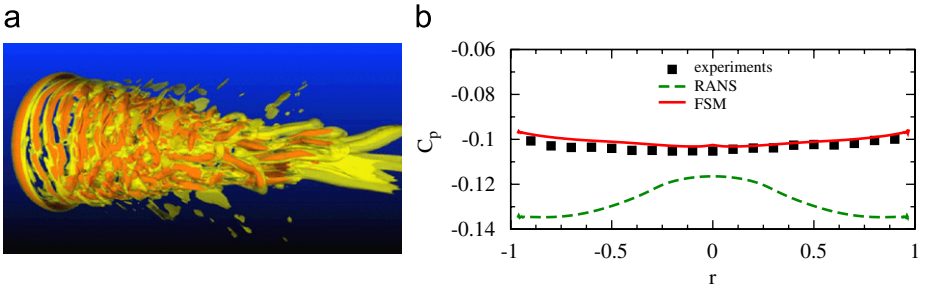

Fig. 9. Supersonic base flow at $Re_D = 3,300,000$ and $Ma = 2.46$ computed using FSM with $\beta = 0.001$ and $n = 1$. (a) Vorticity contours; (b) base-pressure coefficient (courtesy of R.D. Sandberg).

crucial to the simulation outcome. The latter is particularly true for laminar–turbulent transition where DNS-like resolution is required at locations where the flow structures arise. In FSM for cases like those discussed above, it is frequently beneficial to purposely set f_Δ to 1 or to 0. The former was used to impose a pure RANS simulation along the body in the second example, the second may be an option to enhance transition of the FSM solution to a fully turbulent state but was not applied above.

3.2. A weighted sum of LES and RANS model

A simple way to combine two distinct turbulence models into a hybrid model is to apply a blending of the form

$$\phi^{\text{hybrid}} = f\phi^{\text{RANS}} + (1-f)\phi^{\text{LES}} \quad \text{with } 0 \leqslant f \leqslant 1, \tag{14}$$

where ϕ represents the quantity to be merged. It can be a model term in the momentum equation such as ν_t or a term in a secondary equation of the turbulence model. The blending factor f is a continuous function in space and time, commonly chosen in an *ad hoc* manner and calibrated empirically. The factors f and $(1-f)$ constitute a partition of unity since they add up to 1. One example of such a method for deriving hybrid LES/RANS models is discussed in the following.

3.2.1. Description of the method

The shear-stress transport (SST) turbulence model of Menter [62] can be used as a basis for constructing a hybrid LES/RANS method. For the SST, two RANS models are blended: the K–ω model near walls to a K–ε model farther away. For the hybrid method [63,64], the K–ε RANS-model is replaced by an SGS-model for LES using an equation for the subgrid kinetic energy. The resulting ν_t in (10) is then determined as

$$\nu_t = f\nu_t^{\text{RANS}} + (1-f)\nu_t^{\text{LES}} = f\frac{K}{\omega} + (1-f)C_s\sqrt{K}\Delta, \tag{15}$$

where C_s was chosen as 0.01. Furthermore, f is a modification of the SST-blending function, i.e. a hyperbolic tangent function depending on wall distance d and on solution-dependent parameters (K and ω):

$$f = \tanh(\eta^4) \quad \text{with} \quad \eta = \frac{1}{\omega}\max\left\{\frac{500\nu}{d^2}; \frac{\sqrt{K}}{C_\mu d}\right\}, \tag{16}$$

where C_μ is the constant of the SGS model. In addition to using the blended ν_t of (15) in the production and turbulent diffusion terms, in the equation for K also the dissipation rate is blended by

$$\begin{aligned}\varepsilon &= f\varepsilon^{\text{RANS}} + (1-f)\varepsilon^{\text{LES}} \\ &= f\beta^* K\omega + (1-f)C_s\frac{K^{3/2}}{\Delta},\end{aligned} \tag{17}$$

where β^* and C_s are constants from the original RANS and LES closures, respectively. For $1/\omega$ in (16), either a blending similar to (17) or the unmodified result from the ω-equation can be used. Variations of the blending function were proposed in [65] with and without explicit dependencies on the grid size and the wall distance. In addition, a different underlying RANS model was employed. However, tests did not reveal a superiority of a specific form over another.

3.2.2. Sample applications

The resulting model was tested for predicting the unsteady flow over a ramped cavity with moderate success. The results obtained with the hybrid method were better than those of pure RANS or no-model simulations on the same grid. DES, based on both the Spalart–Allmaras and the SST model (cf. Section 4.1) were also tested but yielded only steady results for the grid employed. Note that the method described here is distinct from DES using SST blending discussed below. For the latter, only the length scale in the dissipation term of the model is switched, whereas the definition of the eddy viscosity itself is left unchanged.

3.2.3. Assessment

In general, blending of LES and RANS with (14) can lead to the generation of unphysical flow structures. For example, Baggett [66] showed that near walls an artificial cycle is invoked due to such blending which generates larger-than-physical streamwise streaks and vortices. These "super-streaks" will be encountered again below in Section 4.1.3 in connection with the gray zone of DES. A possible explanation for these artifacts is the so-called modeled stress depletion (MSD) [67]. For MSD, in a transition region between RANS and LES, modeled stresses in a simulation have been reduced (here, by the blending), whereas the resolved stresses also included in the blending have not yet reached the equivalent higher values. If this is the case, mean flow profiles show artifacts such as spurious buffer layers.

In the limit of vanishing extent of the blending region, the blending function f approaches a step function. This turns the hybrid method into a simple interfacing of existing models as described in Section 4 below. Since the weighted sum in (15) can be considerably easier to implement into existing flow solvers than explicit interfaces, it may be considered as an alternative to some of these methods. However, regarding the quality of the solution, trust issues similar as for the URANS approach mentioned in Section 2.1 always remain.

4. Interfacing RANS and LES models

4.1. Detached eddy simulation (DES)

4.1.1. Description of the method

Spalart and Allmaras [68] devised a one-equation RANS model employing a transport equation for the eddy viscosity. More precisely, the governing equation is

$$\begin{aligned}\partial_t\tilde{\nu} + \langle u_j\rangle\partial_{x_j}\tilde{\nu} = c_{b1}\tilde{S}\tilde{\nu} + \frac{1}{\sigma_{\tilde{\nu}}}\Big[\partial_{x_j}\left((\nu+\tilde{\nu})\partial_{x_j}\tilde{\nu}\right) \\ + c_{b2}(\partial_{x_j}\tilde{\nu})^2\Big] - c_{w1}f_w\left(\frac{\tilde{\nu}}{d}\right)^2.\end{aligned} \tag{18}$$

for $\tilde{\nu} = \nu_t/f_{v1}(y^+)$ where f_{v1} is chosen such that $\tilde{\nu}\sim y$ in the proximity of walls. Coefficients and blending functions can be found in the original paper [68] or in other articles on DES.[2]

Spalart et al. [11] then applied the following modification. The last term in (18) represents a destruction term for $\tilde{\nu}$ depending on the wall distance d. This physical length scale can be replaced by a length scale $C_{\text{DES}}\Delta$ involving the step size of the grid Δ and the model constant C_{DES}. Hence, the Spalart-Allmaras model turns into an LES one-equation SGS model. A reduced length scale increases the destruction term and hence yields a reduced eddy viscosity. The authors specifically chose

$$\Delta = \max\{\Delta_x; \Delta_y; \Delta_z\}, \tag{19}$$

and calibrated the constant to $C_{\text{DES}} = 0.65$ by means of isotropic turbulence [69]. Lower values have been used by others, presumably to compensate for numerical diffusion [34]. The second step concerns near-wall flows. In fact, d is replaced with

$$\tilde{d} = \min\{d; C_{\text{DES}}\Delta\}, \tag{20}$$

[2] Note a typographical error in [68]: c_{w1} should read $c_{w1} = c_{b1}/\kappa^2 + (1 + c_{b2})/\sigma$ with κ being squared.

which is natural, since near the wall the length scale should not increase beyond the RANS value. Fig. 11 illustrates the situation. Close to the wall, where $d<C_{DES}\Delta$, the model employed is the original RANS model. Away from the wall, were $d>C_{DES}\Delta$, the model turns into an SGS model. The transition in ν_t is continuous and smooth since only a source term in the auxiliary equation changes smoothly. The fact that a RANS model term is used, however does not preclude the flow field from becoming unsteady. In fact, even with stationary statistics the computed DES solution generally is unsteady near the wall due to the fluctuations in the outer flow.

The authors coined the term detached eddy simulation (DES) for this approach as it is meant to blend an LES of the outer flow, resolving the detached eddies far from any boundary in an LES-like manner, while using a RANS model for the flow near the wall. The latter is aimed at yielding a suitable description of the near-wall flow in a statistical sense which only requires a fine grid in the wall-normal direction but can be used with a coarse grid in the tangential directions. The switch between the two approaches is accomplished by an automated criterion and relieves the user from its specification.

Eq. (19) is based on the argument that with LES the coarsest step size determines the resolvable vortices. This issue is rather an LES than an LES/RANS issue and discussed in Section 2.2 above, but it also influences the position of the LES/RANS interface. Good arguments for (19) can be found in [70]. Furthermore, one is on the safe side as explained above. In [71] a quadratic mean was used to determine Δ yielding only slight changes in the result.

The basic idea of DES can be combined with other RANS models as well. A candidate is the SST model [62] which is widely applied nowadays. For this DES–SST, the length scale in the dissipation term of the K-equation can be modified to $\ell_{DES}=\min\{\ell_{SST};C_{DES}\Delta\}$. The model parameter can be determined via $C_{DES}=(1-f_1)C_{DES}^{K-\varepsilon}+f_1C_{DES}^{K-\omega}$ using the blending function f_1 of the original SST model with $C_{DES}^{K-\varepsilon}=0.61$ and $C_{DES}^{K-\omega}=0.78$ [72].

4.1.2. Applications to flows with detached eddies

The first applications of DES were concerned with high-lift airfoils. In [69] the flow around a NACA-0012 airfoil was computed with $Re=10^5$ for angles of attack $\alpha=0^\circ\ldots90^\circ$. For small α, the solution was steady and corresponded entirely to the RANS mode. For higher α, massive separation developed on the suction side and unsteady vortices were observed. The results substantially improved upon two-dimensional URANS. At high angle of attack the separation point is more or less fixed by the geometry and the flow in the massive separation region is insensitive to the details of the near-wall flow. This application hence corresponds to the design situation of DES. Other applications of this type are the computation of the flow around a simplified landing gear [72,73] or the flow around a fighter at high angle of attack [74]. With the latter, only global values such as lift and drag coefficients were compared to experimental values. In fact, many published DES results show qualitative data in terms of flow structures but rarely quantitative comparisons. There are situations, however, where this is relevant and answers a precise question. An illustrative example is the flow around an entire C-130 airplane conducted in [75] with the purpose of clarifying why parachutists were exposed to gusts when jumping off the plane. The DES showed a critical vortex structure close to the door in question without quantitative predictions reported. A review on DES for bluff body flows is given in [76].

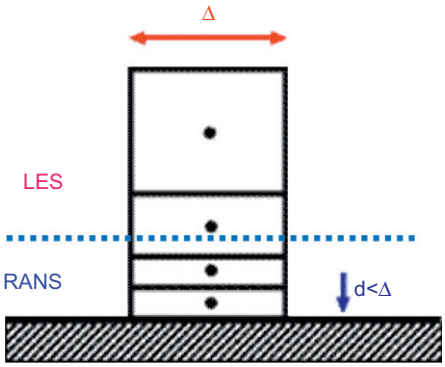

Fig. 11. Illustration of the switch between RANS and LES in the traditional DES approach as discussed in the text.

4.1.3. DES as a wall model

With massive separation the coupling between the LES and the RANS zone in DES is weak or rather uninfluential for the global result of the simulation. When the flow is attached to a wall the situation is different. In fact, one can attempt to use DES as a wall model. Given a particular grid, the point where $d=C_{DES}\Delta$ is fixed, and hence the interface between the region where an LES and where a RANS model is employed. Due to the combination of a higher RANS eddy viscosity and the trigger from outer fluctuations, the solution in the RANS region exhibits weak oscillations. In the LES region, the solution has to become unsteady. In order to be a true LES, an amount of 80% or so of the kinetic energy of the fluctuations should be resolved. The transition between these regions is critical and takes place in a "gray area" [69]. Fluctuations need to be generated by some sort of instability [34]. For an attached boundary layer, however, this does not happen vigorously enough if the method is left alone, as shown by Nikitin et al. [77]. They conducted simulations of plane channel flow at various Reynolds numbers to assess this issue. The step size of the grid in the spanwise direction was deliberately chosen to be large, up to $\Delta_z^+=8000$, while maintaining $\Delta_y^+\leqslant1$ near the wall by means of stretching. The results exhibit a spurious buffer layer with "super-streaks" at the location where fluctuations in the solution are naturally created. This location is determined by the grid and is found at a larger distance from the wall.

4.1.4. Enhancements of the basic method

Piomelli et al. [71] tackled the problem of the spurious buffer layer by supplementing the method with a stochastic forcing term. It introduces turbulent kinetic energy and enhances the generation of fluctuations in the LES region close to the interface. Super-streaks and the resulting unphysical behavior can be avoided in this manner. This ad hoc forcing was performed for each component of the momentum equation within a region surrounding the interface using a smooth envelope. A substantial improvement of the mean velocity profile was observed so that this approach seems very promising.

Another modification of the original DES formulation attempts to avoid unphysical behavior in attached boundary layers by eliminating the gray zone with MSD altogether or at least severely shrinking its size. To this end, Spalart et al. [67] added a function f_d to the definition of the dissipation length-scale in (20):

$$\tilde{d}=d-f_d\max\{0;d-C_{DES}\Delta\},\tag{21}$$

where

$$f_d=1-\tanh[(8r_d)^3]\tag{22}$$

$$\text{and } r_d=\frac{\nu_t+\nu}{\sqrt{\partial_{x_j}\langle u_i\rangle\partial_{x_j}\langle u_i\rangle\kappa^2d^2}}=\frac{\tilde{\nu}}{S\kappa^2d^2}.\tag{23}$$

The function f_d was designed and calibrated such that DES solves attached boundary layers in RANS mode no matter what grid resolution is chosen. Intended to prevent DES from a too early

switch to LES mode, the modified version was called delayed detached eddy simulation (DDES). It was tested for an array of prototypical flows and was proclaimed as the new standard. The change from (20) to (21) has, however, some serious repercussions. In DDES, a dependency on the solution and, therefore, also on time has entered $\tilde{d}$. Although this can be attractive in general, it will be seen below that, for DDES, this can result in a sensitivity of mean flow values to the IC which is clearly undesirable.

4.1.5. DES and DDES for the flow over periodic hills

The flow over periodic hills proposed in [78] has become a standard benchmark case for testing turbulence modeling strategies [79]. It was specifically designed to facilitate economical computational studies such that periodic boundary conditions in the streamwise and lateral directions were used and the hills were placed inside a channel. The Reynolds number based on bulk velocity and hill height was chosen as $Re = 10,595$ to allow for well-resolved LES benchmark data and at the same time to deliver a separated and fully turbulent flow suitable to test RANS model predictions. Lately, it has also been used to evaluate hybrid LES/RANS methods in several papers. Šarić et al. [80] scrutinized DES with this configuration and compared the results to LES and other hybrid methods for different grids and interface locations. In the following sections this flow is used whenever data are available to assess the performance of methods facilitating mutual comparison. Here, we start with own DES and DDES performed on a grid with roughly one million cells. Reference data from a recent LES with a grid of 12 million points [81] are used for comparison. Note that RANS methods have considerable difficulties for this type of flow as observed with a single hill in [2] or the periodic case in [4]. A glimpse of these problems is provided by the third zone in Fig. 23b below, where the RANS solution exhibits a substantially longer reattachment length than the reference data.

The ICs for the DDES computation were chosen as an ordinary user might naturally choose them. A realistic procedure is that first a standard RANS simulation is performed in order to get an idea about the flow field, the solution of which is then used as IC for an unsteady simulation. The second case reported here was started from an arbitrary initialization, here specifically $u = 1$ and $v = w = 0$ everywhere yielding vigorous fluctuations in the initial phase of the computation. A third choice was also tested, the use of instantaneous data available from a previous simulation. These results are identical to the second simulation and hence not shown here. Averages were determined over at least 800 time units h/U_b, such that the sampling error is negligible.

In Fig. 12, instantaneous contours of the streamwise velocity are reported. They show that all simulations yield a similar unsteady flow field. The large amount of fine-scale fluctuations in these graphs proves that remote from the walls (D)DES exhibits LES character as discussed above. On the other hand, it is not possible to infer from Fig. 12b that DES under similar conditions exhibits less fine-scale structures than DDES due to the intermittent nature of the large-scale structures [79]. Fig. 13 therefore provides sample results for statistical quantities selected to highlight the differences between the results. A location within the region of mean separation was chosen $x/h = 2$, where h is the height of the hills. The mean streamwise velocity profiles agree fairly well and overall the results are more than adequate, in particular considering RANS results and other hybrid methods discussed below. However, most of the flow field is solved in LES mode and traditional LES on the same grid delivers results of a similar quality [82,80]. Differences between the variants of DES, if they exist, are mostly visible near walls. At the upper wall, an attached boundary layer exists and the interface of the classical DES is slightly inside the boundary layer. DDES switches therefore somewhat later, yielding lower values of resolved wall shear-stress. However, depending on the IC, the resolved turbulent longitudinal stresses of the two DDES differ by roughly 50% which is somewhat disturbing. Even worse, at the lower wall, the DDES with RANS IC shows an unphysical pronounced near-wall peak and both normal stress components deviate in most of the flow field from the other DDES and the DES solution. Such a sensitivity of DDES toward variations in the IC was conjectured in [67], but in the present case, visual interpretation of the instantaneous solution does not point to this issue as suggested in the reference.

4.1.6. Assessment

Spalart stated in [34]: "It is a beauty and a danger of DES that it is robust to grid spacings that are too coarse for accuracy." In fact, many early results using DES were obtained on extremely coarse grids. This applies particularly to the spanwise direction of geometries invariant in this direction [83]. Practitioners are used

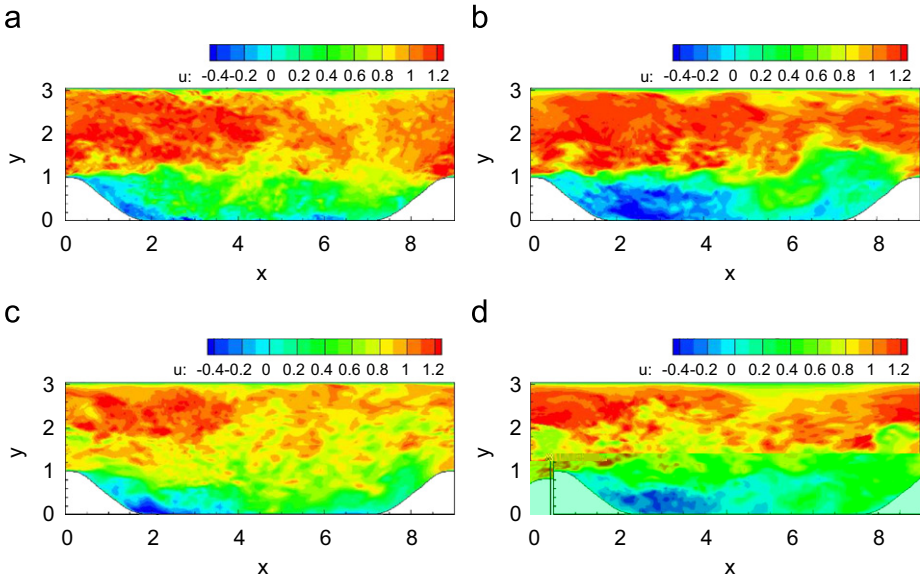

Fig. 12. Contours of instantaneous streamwise velocity for the flow over periodic hills at arbitrary instants in time. (a) Reference LES [81]; (b) DES; (c) DDES (IC: U = 1); (d) DDES (IC: RANS).

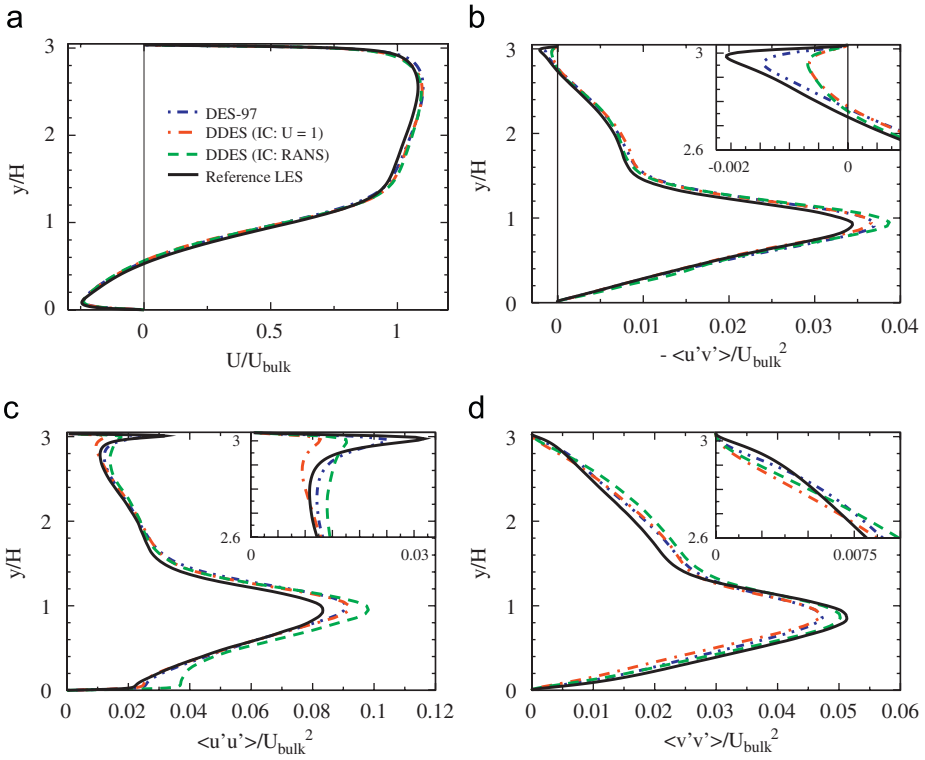

Fig. 13. Results from DES and DDES with two different initial conditions at $x = 2$. (a) Mean streamwise velocity; (b) resolved turbulent shear stresses; (c) resolved turbulent longitudinal stresses; (d) resolved turbulent wall-normal stresses.

to obey rules of near-wall resolution in terms of the wall distance of the first grid point from the wall. With DES, however, an LES-type simulation is performed in the outer flow. Hence, the grid has to be sufficiently fine, also in the spanwise direction, to capture the kinematics of these vortices [84,85]. With under-resolved simulations the behavior becomes highly nonlinear such that results even for the mean flow [86] can deteriorate if the grid is refined.

The DES of the subcritical flow around a circular cylinder at $Re = 140,000$ in [69] resulted in a separating shear layer substantially thicker than in the experiment and in LES of the same flow [87]. The transition process in this shear layer, however, determines the near wake to a substantial extent and is not adequately captured when the flow field is smoothed and a dissipative SGS model is used. This yielded a recirculation length of the DES markedly different from the experimental value [69]. With such transitional regions the only reasonable strategy to-date seems to be an increase in the resolution up to near-DNS spacing [88,34]. In this situation, DES as well as LES are problematic approaches. If the transition by itself is not of interest, addition of stochastic forcing as mentioned above might be a strategy to alleviate this problem, but it seems delicate in its tuning to a given situation. Also note that large time steps can have a similar excessive damping effect as too coarse resolution in space. A detailed discussion and helpful guidelines w.r.t. computational grid requirements for DES can be found in [34].

Finally, the assessment of DES solutions should be mentioned. In fact, many DES in the literature are inspected visually, relating a higher amount of unsteadiness to a better simulation [34]. This might be suitable for some situations as mentioned above. In general, quantitative validation should still be performed. It is then necessary to account for the modeled fluctuations in the RANS and the gray zone and to add them to the resolved ones.

According to the above experience, it seems advisable to perform DDES with two different ICs in order to assess their impact on the overall flow field. For the hill flow no clear superiority over classical DES was attained, but results by the authors of the method showed that the goal of removing the issue of MSD was attained. Application to a wider range of flows is certainly necessary.

4.2. Layering RANS and LES

As pointed out in Section 1, the resolution requirements near walls pose a major challenge to the application of LES to complex flows. This challenge is the main motivation for those hybrid methods bridging the region between the wall and the LES domain by a layer computed with a RANS model, hence the name two-layer model in some publications. LES and RANS solutions are coupled at an interface which may be either pre-defined (*hard interface*) or solution-dependent (*soft interface*). Apart from the soft/hard distinction, different hybrid models employ different RANS and LES models, but moreover they distinguish themselves by the quantities which are explicitly coupled, and how these are coupled. With this approach, the models themselves or quantities directly used in the models are matched at an interface and not a term in the transport equation of the turbulence model, as with DES or DDES.

4.2.1. Definition of the interface location

An integral part of any two-layer model is the definition of an interface location y^* in a suitably chosen coordinate system. Pre-defined hard interfaces are commonly placed by choosing a grid line or a distance from the wall, e.g. $y^* = y_{\text{int}}$. Considering the evolution of the flow in the downstream direction, some researchers sought for improvements of two-layer models by

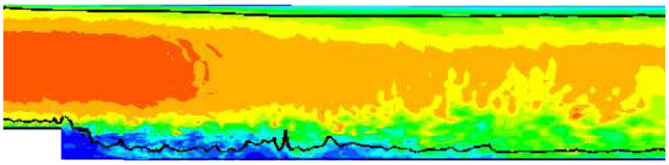

Fig. 14. Interface location and contours of instantaneous velocity for the turbulent flow over a backward-facing step using a soft-interfaced two-layer hybrid LES/RANS model ($K^* = 0.2$) [90].

employing soft interfaces that keep on adjusting with the flow, so that the interface position y^* changes with time. An additional benefit of such a method is that the user is relieved from deciding on a good switching location prior to the simulation. One possibility to achieve this is to specify the wall-distance in a solution-dependent coordinate system. The switching between LES and RANS can then be placed at the same location $y^* = \text{const.}$ in this coordinate. Using the coordinate in near-wall scaling

$$y^* = y^+_{\text{int}} = \frac{y_{\text{int}} u_\tau}{\nu} \tag{24}$$

is one example ($u_\tau = \sqrt{\langle \tau_{\text{wall}} \rangle / \rho}$). For attached turbulent flows, a location in the logarithmic layer of the streamwise velocity profile might be chosen, e.g. $y^+ = 100$.

For separated flows, τ_{wall} vanishes at separation and reattachment points making this coordinate system obsolete, although this can be handled easily by technical adjustments. Alternatively, the modeled or total turbulent kinetic energy can be used to define the switching point as for the approach of Breuer et al. [89], where

$$y^* = \frac{y_{\text{int}} \sqrt{K}}{\nu}. \tag{25}$$

Another switching criterion suggested by Kniesner et al. [90] follows the idea that, for LES to work, a sizeable amount of the turbulent kinetic energy must be resolved. This leads to the use of the ratio of modeled kinetic energy K_τ to total turbulent kinetic energy

$$K^* = \left\langle \frac{K_\tau}{K_\tau + 1/2(\overline{u}'\overline{u}' + \overline{v}'\overline{v}' + \overline{w}'\overline{w}')} \right\rangle. \tag{26}$$

The averaging operation was carried out in homogeneous directions. Then, if K^* exceeds a threshold, say 20%, the interface is moved away from the wall and vice versa. Furthermore, this criterion ensures that for well-resolved simulations the RANS layer eventually vanishes whereas for very coarse simulations RANS prevails. A typical example of the distribution of such a soft interface is given in Fig. 14 for the turbulent flow over a backward-facing step. There $K^* = 0.2$ was chosen yielding an interface location of $y^+ \approx 230$.

4.2.2. Description of methods

Cabot and Moin [91] and Piomelli and Balaras [92] reviewed approaches to wall modeling in LES. Some of these employ a boundary-layer type Reynolds-averaged transport equation solved in the interior of the near-wall grid cell on an embedded grid, e.g. in [93]. A hierarchy of such models is proposed in [16]. As discussed above, such models also contain some sort of hybrid LES/RANS coupling, and since the position of the interface is fixed by the grid, this is a hard interface.

Common to the general layered models to be discussed in this section is the continuous computation of a quantity ϕ (or several quantities) across the interface positioned at y^*. For the corresponding transport equations, i.e. the momentum equation and selected model transport equations, this yields

$$\langle \phi \rangle(t, y^*) = \overline{\phi}(t, y^*). \tag{27}$$

Since the RANS models are operated in unsteady mode due to the coupling with the time-dependent LES, $\langle \phi \rangle$ is generally time-dependent. This raises the issue of compliance with the original definition of the averaging and filtering operations. For equations that are valid only in one layer, explicit boundary conditions need to be set, see below.

Davidson and Peng [94] used RANS with the K–ω model near the wall and a one-equation LES model based on K_τ. The ω-equation was solved only in the RANS layer with the boundary condition

$$\left. \frac{\partial \omega}{\partial y} \right|_{y^*} = 0 \tag{28}$$

at the interface. The K-equation turned into the K_τ-equation at the interface and was solved continuously. The interface location was chosen at a certain grid line.

Temmerman et al. [95] coupled a one-equation RANS model near the wall which uses a K-equation with a one-equation LES model based on K_τ, again implicitly enforcing $K_\tau = K$ at the merging points. To enforce

$$\nu_t^{\text{RANS}} = \nu_t^{\text{LES}} \tag{29}$$

at the interface in addition, C_μ in the RANS layer was modified using an empirical blending function:

$$C_\mu = 0.09 + (C_\mu^* - 0.09) \frac{1 - \exp(-y/\Delta)}{1 - \exp(-y^*/\Delta^*)}. \tag{30}$$

Again, the asterisk denotes values at the interface which was identified with a certain grid line.

Kniesner et al. [90] matched various K–ε RANS models with LES employing either a Smagorinsky or the one-equation Yoshizawa SGS model [96]. For the latter, the transport equation for K (or K_τ) was solved continuously. Additional boundary conditions for the RANS equations were then obtained from the LES data. For the Smagorinsky model they read

$$K = \frac{(C_S \Delta)^2 S^2}{0.3} \quad \text{and} \quad \varepsilon = (C_s \Delta)^2 S^3 \tag{31}$$

and for the Yoshizawa model

$$\varepsilon = \frac{C_\varepsilon K_\tau^{3/2}}{\Delta}. \tag{32}$$

Here, S is the magnitude of the resolved strain-rate tensor, Δ is a representative scale for the grid, while C_S and C_ε are model constants. The interface location was determined using (26).

Breuer et al. [89] matched RANS and LES based on one-equation models for K and K_τ. No explicit coupling conditions were needed to be specified. Two different RANS models were tested: A linear near-wall model based on $\sqrt{\overline{v^2}}$ (but expressed in form of K) and a nonlinear explicit algebraic Reynolds stress model that is able to account for anisotropies, streamline curvature and redistribution of energy among different Reynolds stress components. For this method, the interface was determined employing (25).

A mismatch of the slopes of the logarithmic velocity profile for turbulent channel flows is usually visible when using the above two-layer approaches as described so far. Hamba [97] demonstrated that this is indeed a fundamental problem independent of the type of models matched, the method of interfacing, and whether the RANS region is between the LES and the wall or vice versa. He conjectured that the mismatch is related to a rapid change in the length scales of the RANS and LES models. By allowing for a discontinuous change of the length scales and using

information from DNS data he was able to eliminate the mismatch. Since this is unpractical in a realistic setting, he suggests to use a linear blending function for adjusting the turbulent dissipation rate used in the RANS and LES models over a blending region within the logarithmic region of the velocity profile. However, the mismatch remained, albeit with a smaller magnitude than before.

4.2.3. Application to the flow over periodic hills

The flow over periodic hills has been used to scrutinize some of the two-layer hybrid models discussed above. In [94] the hard interface was located at the 13th grid point from the wall, roughly at $y \approx 0.1$. Kinks in the mean flow profiles at the interface occurred so that the result (not shown here) was unsatisfactory. However, since only 200,000 cells were employed, the coarseness of the computational mesh might have been too aggressive for a fair assessment. In [80], reasonable results for the hill flow were obtained using DES and LES on coarse grids with 480,000 cells.

In Fig. 15, streamlines of the mean flow are shown and reattachment lengths are given for the reference LES (12 million cells), the hard-interfaced method of Temmerman et al. [95] (400,000 cells) and the two soft-interfaced hybrid models of Breuer et al. [89] (one million cells). All results are acceptable, in particular bearing in mind the difficulties with RANS for this flow. The hard-interface model exhibits the poorest performance, for both attempted switching locations at the 13th and the 18th grid line (only the latter is shown here). However, this simulation used also a coarser grid than the soft-interface methods such that a direct comparison is somewhat difficult to make. Such a comparison is possible for the soft-interface models. Here, the use of a nonlinear relationship between turbulent stresses and mean flow field clearly pays off. Two reasons for this are possible. One is that the anisotropies near the wall matter. Another is that at reattachment and separation points the normal stress components play an important role. Probably both points are valid here. In Fig. 16, the above impressions are confirmed with mean streamwise velocity profiles at chosen locations in the flow.

4.2.4. Assessment and comparison with other near-wall treatments

Hybrid methods matching RANS with LES in wall-parallel layers have been developed and tested for more than a decade now. Albeit the methods have been continuously improved, they still have not met with the success hoped for. The unphysical deviations in mean flow profiles occurring at the interface for simple configurations like turbulent channel flow, as observed in [77], are casting doubts on the quality of predictions obtained with such approaches, in particular for applications where the near-wall flow plays an important role.

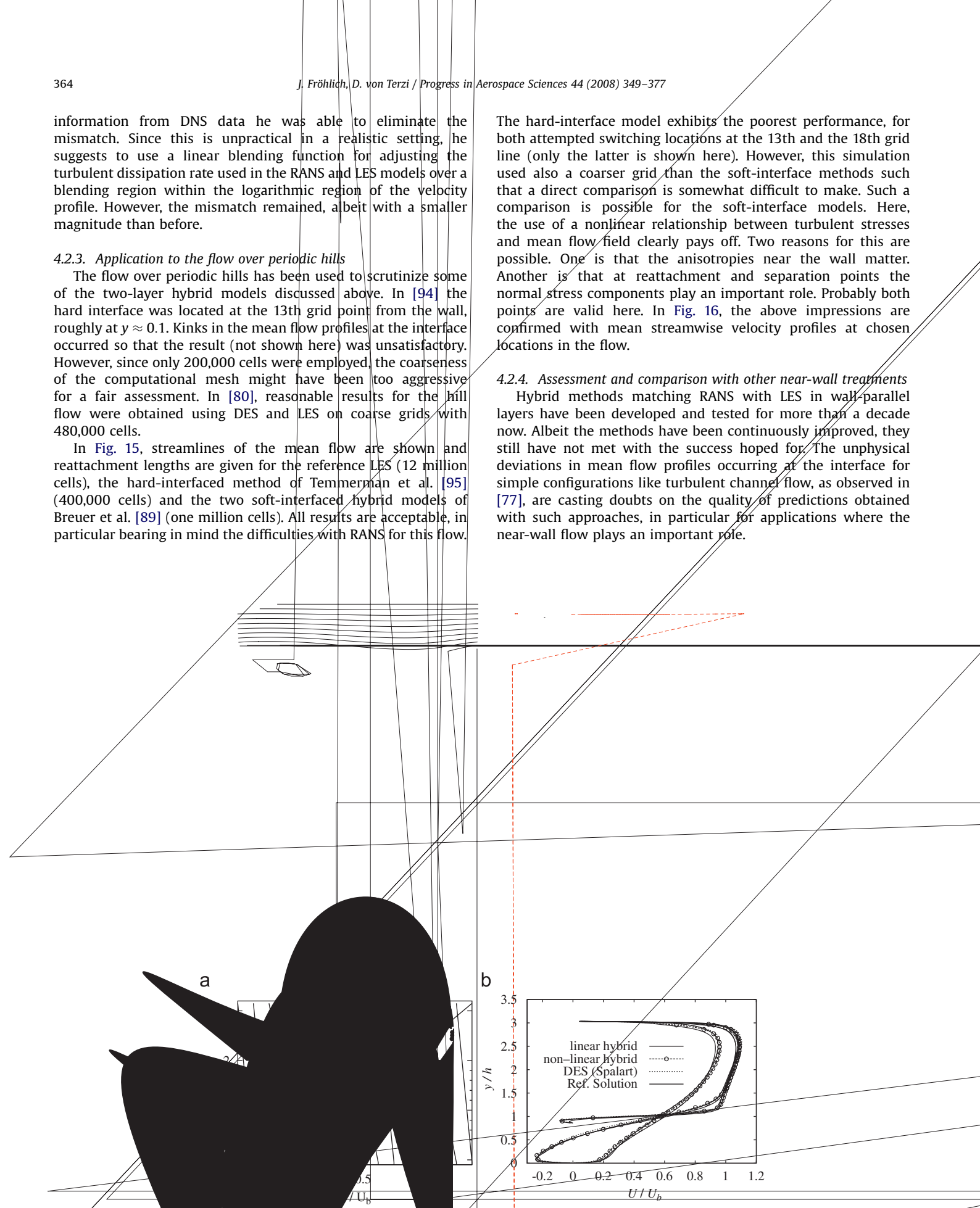

Fig. 16. Mean streamwise velocity profiles for the flow over periodic hills using hard [95] and soft [89] interfaced two-layer hybrids. (a) Hard interface, $x = 2$; (b) soft interface, $x = 0.5$, 2 and 6.

In Section 2.5, when discussing tangential coupling near walls, the possibility of deviations at the interface was mentioned and attributed to a combination of performing RANS calculations for flows with steady statistics, but unsteady boundary conditions (provided by the LES layer) and, as a consequence, some double-accounting of fluctuations resolved by the URANS, but also included in the RANS model. A possible remedy is presented in Section 6.3 by subtraction of the resolved stresses from the RANS model in the wall layer.

In the literature, another point of view is often taken in order to explain the observed deficiencies: the lack of physical flow structures for the LES side of the interfaces. With this in mind, the supply of additional fluctuations in the vicinity of the interface is recommended to alleviate the problem. To this end, Quéméré and Sagaut [49] suggested to couple only the mean velocity fields and to generate fluctuations by copying them from the LES domain. For this approach, the models are decoupled and the solution is matched. It therefore is a segregated approach that is discussed in Section 5.2 below.

Alternatively, in the context of DES, Piomelli et al. [71] (see Section 4.1.4) suggested and successfully tested the use of explicit forcing terms in the momentum equations in order to generate smoothed random fluctuations under the constraint of being divergence-free. This approach is readily applicable to two-layer models and has already been tested for several of the two-layer models from above, with some modifications, e.g. by Davidson and Dahlström [98] and Kniesner et al. [90]. Results of the latter are shown in Fig. 17 clearly demonstrating the feasibility and promise of such a technique. How the amplitudes of the forcing have to be adjusted to individual cases is still an open question.

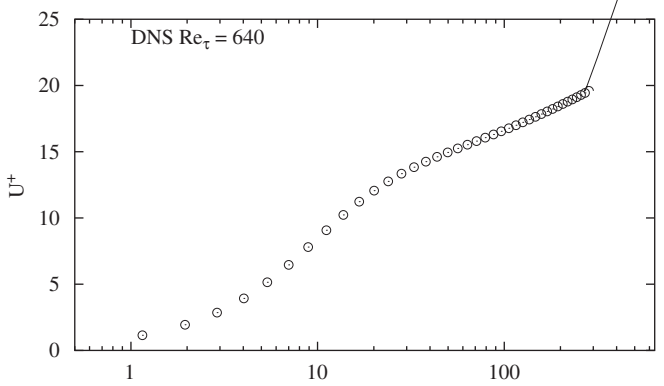

4.3. RANS-limited LES

4.3.1. Description of the method

In the literature renormalization group (RNG) theory was used to determine coefficients for various turbulence models, in particular a variant of the K–ε RANS model [99]. The strategy for deriving model equations employs an iteration in spectral space. Small wavenumber bands beyond a cutoff are successively eliminated and accounted for by modifying the viscosity. Upon completion of the procedure, a RANS model is obtained with an eddy viscosity only depending on K and ε. If the procedure is stopped at some finite wavenumber $2\pi/\Delta$ related to the step size of the computational grid, an LES model is obtained. The K and ε equations then turn into equations their SGS counterparts K_τ and ε_τ. Depending on the choice of Δ the whole range from viscous scales, the DNS-limit, to the integral length-scale of turbulence, the RANS-limit can be covered. However, in order to close unknown terms, restrictions due to further modeling assumptions enter this approach which are delicate.

Such a unified turbulence model was constructed by DeLanghe et al. [100,101]. The equations for K_τ and ε_τ are solved in the entire domain, but in region in LES-mode only one of them is employed for SGS modeling. Interestingly, it is the equation for the SGS dissipation rate ε_τ which is retained for the LES mode to determine:

$$\nu_t^{\mathrm{LES}} = C_\mu \varepsilon_\tau^{1/3} \Delta^{4/3}, \tag{33}$$

where C_μ is a constant. The equation for K_τ is needed to estimate the integral length-scale

$$\ell = \frac{K_\tau^{3/2}}{\varepsilon_\tau} \tag{34}$$

as a measure to determine if locally the coarse-grid (RANS) limit is reached. The hybrid method is then obtained by replacing Δ with ℓ in (33) whenever and wherever $\Delta \geqslant \ell$. This is equivalent to replacing ν_t^{LES} with

$$\nu_t^{\mathrm{RANS}} = C_\mu \frac{k^{3/2}}{\varepsilon}, \tag{35}$$

since $K = K_\tau$ and $\varepsilon = \varepsilon_\tau$ is assumed for $\Delta \geqslant \ell$. The interface between LES and RANS models is hence defined by instantaneous locations where $\nu_t^{\mathrm{RANS}} = \nu_t^{\mathrm{LES}}$. It is solution-dependent. A low Reynolds number version with near-wall modeling of the hybrid method can be found in [102].

4.3.2. Sample applications

The model was tested for the flow over periodic hills, a backward-facing step, a sudden pipe expansion, and a plane channel. In Fig. 18 instantaneous contours of the streamwise velocity component are shown for the hill flow. Only very large-scale unsteady motion is visible even though the simulation was

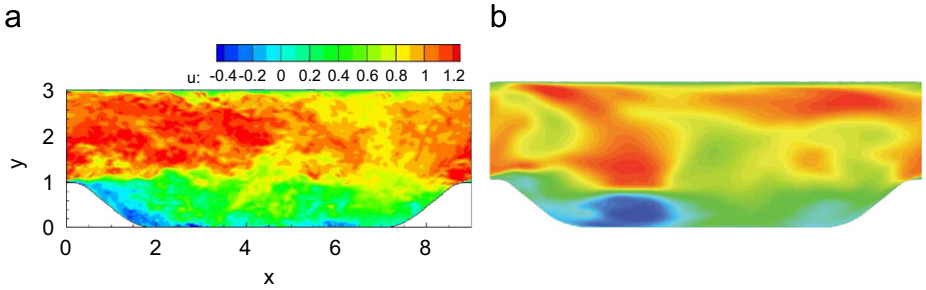

Fig. 18. Contours of instantaneous velocity for the flow over periodic hills obtained by RANS-limited LES [102]. (a) Reference LES [81]; (b) RNG-hybrid.

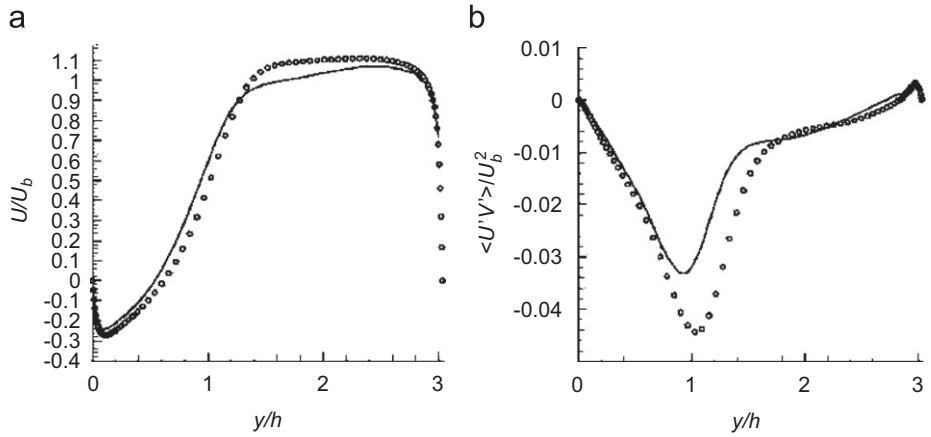

Fig. 19. RANS-limited LES results from [102] for the flow over periodic hills at $x = 2$ compared to highly resolved LES from [79]. (a) Mean streamwise velocity; (b) resolved turbulent shear stresses.

in LES mode almost everywhere in the flow field. In Fig. 19, mean velocity and resolved shear-stress profiles at a location inside the region of mean separation are compared to LES reference data from [79]. Albeit qualitatively correct, the results still leave room for improvement, in particular considering results obtained with other methods (see Section 4.1 or [80], for example). However, the grid employed was coarse and of poor quality with 230,000 cells only.

4.3.3. Assessment

The RNG hybrid model is easily implemented in a flow solver with existing K–ε model. Constructing a one-equation SGS model based on the subgrid-dissipation rate is also very interesting. It is still unclear, however, how this hybrid model performs in a regime where more flow structures are resolved than shown in Fig. 18. The results above seem to exhibit a relatively large value for the eddy viscosity. More studies of the properties of this model and others which are similar would be needed to elucidate this issue.

The underlying idea of the hybrid method discussed above is to locally and instantaneously limit the eddy viscosity of a given LES model by the value of its corresponding RANS model in order to circumvent the problems of classical LES models in the coarse grid limit (see the discussion in Section 2.3). Since many more SGS models are or can be derived from RANS closures, a generalization is obvious, i.e. a hybrid method can be constructed as

$$\phi^{\text{hybrid}} = \min\{\phi^{\text{LES}}; \phi^{\text{RANS}}\}, \tag{36}$$

where ϕ is a modeling quantity for which the RANS value constitutes a maximum, such as ν_t or a length-scale ℓ in the model. The difference w.r.t. DES in Section 4.1 is that, for DES, ℓ^{LES} is limited by ℓ^{RANS} in the dissipation term of the model transport equation whereas, here, the limiting quantity is either the model term itself or a characteristic scale directly used in the constitutive relation of the model.

4.4. Limited numerical scales (LNS)

Inspired by the original proposal of Speziale, Batten et al. [103,104] developed a variant of this approach which they called limited numerical scales (LNS) setting

$$\tau_{ij}^{\text{model}} = \alpha \tau_{ij}^{\text{RANS}} \tag{37}$$

and using a cubic K–ε model for τ_{ij}^{RANS}. Aware of the consistency issue discussed in Section 3.1.2, the authors proposed to use τ_{ij}^{model} instead of τ_{ij}^{RANS} in the transport equations for K and ε. As a consequence, these quantities become K_τ and ε_τ since they are determined as solutions of some sort of subgrid-scale transport equations. Hence τ_{ij}^{RANS} computed with K_τ and ε_τ is turned into a subgrid stress model. Damping this model again results in a "double-damped" τ_{ij}^{model}. To compensate for this, Batten et al. adjusted the contribution function significantly. They termed it latency factor and used

$$\alpha = \frac{\min\{\nu_t^{\text{LES}}; \nu_t^{\text{RANS}}\}}{\nu_t^{\text{RANS}}} \quad \text{hence } 0 \leqslant \frac{\nu_t^{\text{LES}}}{\nu_t^{\text{RANS}}} \leqslant \alpha \leqslant 1. \tag{38}$$

Here, ν_t^{RANS} is the RANS equivalent eddy viscosity obtained by using K_τ and ε_τ in the original RANS definition, while ν_t^{LES} is the eddy viscosity of an LES model of choice. In other words, for sufficiently fine grids, τ_{ij}^{RANS} is scaled down to LES-like values. Batten et al. selected the Smagorinsky model with

$$\nu_t^{\text{LES}} = C_S \Delta^2 S, \tag{39}$$

where $C_S = 0.05$ and

$$\Delta = 2 \max\{\Delta_x; \Delta_y; \Delta_z\}. \tag{40}$$

If τ_{ij}^{RANS} were to be a linear eddy viscosity model, then inserting (38) in (37) and comparing with (36) reveals that LNS would turn FSM into a RANS-limited LES as discussed in Section 4.3. The use of a nonlinear RANS-model, however, leads to modifications in LES-mode, but this characteristic is retained.

LNS still fulfills all the demands on a unified model put forth by Speziale and was applied to an array of test cases with fair success. A particular example is the flow over periodic hills introduced above. On a coarse grid of approximately 600,000 cells adequate results were obtained with a somewhat too long reattachment length [105]. The results were better than for a pure RANS on the two-dimensional version of the same grid. Apart from the consistency issue, which is less traceable here, the remarks made on FSM in Section 3.1 and on the RANS-limited LES still hold.

5. Segregated modeling

Segregated modeling for hybrid LES/RANS methods is based on decomposing the entire domain before starting the simulation into clearly identifiable regions for RANS and LES. The connection between the distinct zones during the simulation is established via explicit coupling of the solution, i.e. velocities and pressure, at

the interfaces. A sketch of such a situation is shown in Fig. 5. This issue has presumably been described in its full generality first by Bertoglio and co-workers [106–108]. Note that for a true LES/RANS hybrid method the coupling has to be two-way with exchange in both directions. Otherwise, the problem is reduced to a standard LES setup, where the RANS solution can be computed *a priori* and only serves to provide better boundary conditions, like in a fairly successful simulation of the flow over the Ahmed body [109].

The aim of segregated modeling is to compute all models in their regime of validity: steady RANS for flows with stationary statistics and unsteady LES with high resolution where it is needed. Therefore one can choose the best suited method for each subdomain without considering their compatibility and without fear of inconsistencies in their use. Furthermore, any gray zone where the model is left alone with generating fluctuations in some transition process is avoided. The price to pay is the need for comparatively complex coupling conditions. For block-structured solvers, however, the routines for data exchange required anyway facilitate a straightforward implementation. Inappropriate coupling conditions lead to contamination of the results in the LES or RANS subdomains. Depending on the type of the interface illustrated in Fig. 5, the requirements on the coupling conditions differ as discussed below.

5.1. Inflow coupling

At inflow-type interfaces, mass, momentum, energy, flow structures, etc. are convected from a RANS region into the subdomain treated by LES. The mean values are provided by the RANS calculation and coupled to the explicitly averaged LES data. If very strong instabilities exist inside the LES domain and the upstream unsteadiness has only little impact on the downstream flow, this might already suffice. An example could be the supersonic baseflow discussed in Section 3.1.3 above. In all other cases, the LES requires the provision of fluctuations at the interface in order to avoid an artificial transition zone in the LES subdomain. To this end, methods applicable for pure LES can be used. Consequently, only a brief overview is given here, referring the reader to the literature for more details, e.g. the articles in the special edition in [110] on this topic or the review in [46].

Two classes of unsteady inflow data can be distinguished: real unsteady flow structures and artificial fluctuations, where the latter can be seen as a model of the first. Real flow structures can be provided in several ways: specifically designed precursor simulations or databases for similar flows with additional adjustment. Synthetic turbulent fluctuations can be obtained by various strategies: proper orthogonal decomposition (POD) modes, Fourier modes, digital filters, random vortices, stochastic forcing, etc. Imposing fluctuations as close as possible to those present in the real flow is crucial. Otherwise they will be damped rapidly, hence failing the purpose of the method.

An example of a synthetic inflow data generation used for the periodic hill flow is given in Fig. 20. A periodic boundary condition providing physical flow structures is compared with random white noise, a vortex method presented by Mathey et al. [108] and a modification of the vortex method implemented in collaboration with the first author [111]. Random noise yields too long a reattachment length. The original vortex method and more so the modified vortex method improve the situation.

The application of a database technique for the generation of unsteady fluctuations at a RANS/LES boundary is illustrated in Fig. 21 for the example of an asymmetric diffuser. The embedded LES is conducted to resolve the region of separated flow whereas two-dimensional RANS is performed in the surrounding domain.

5.2. Outflow coupling

For any RANS zone downstream of an LES zone the primary task of a hybrid LES/RANS coupling at an outflow-type interface is

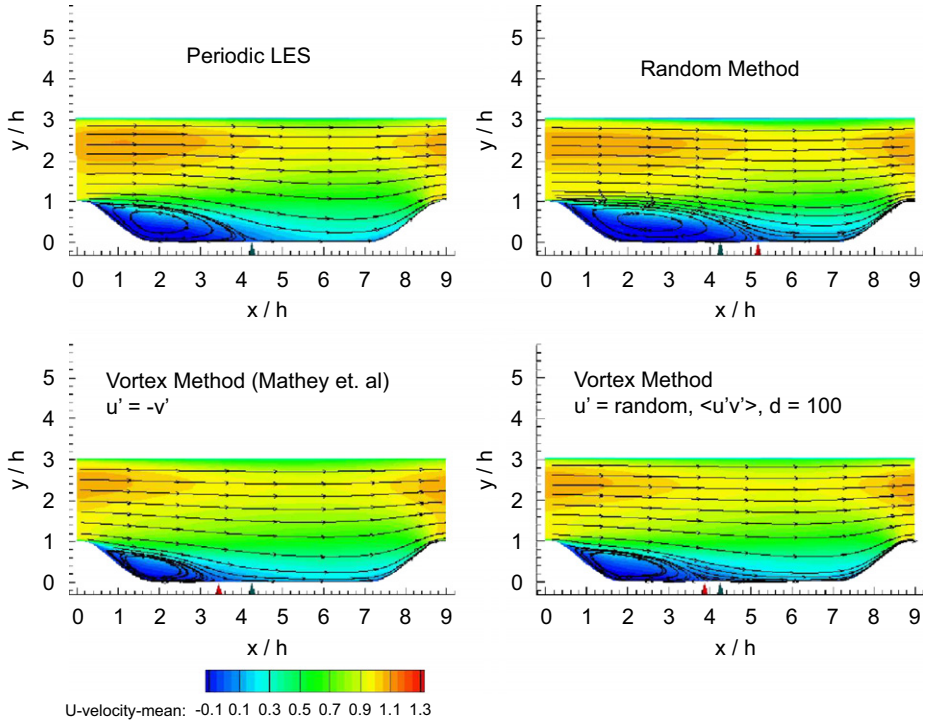

Fig. 20. Unsteady inflow data generation using synthetic flow structures for the flow over periodic hills; the green triangles mark the reference reattachment location whereas the red triangles indicate the achieved one. Plots reproduced from [111].

to propagate mean flow information upstream. At the same time, for flows with stationary statistics, the LES should provide only mean flow data to the RANS domain. Since the LES delivers unsteady data, the interface has to allow for the fluctuations to leave the LES domain without reflections. Several techniques for such a two-way coupling fulfilling these demands have been proposed in the literature.

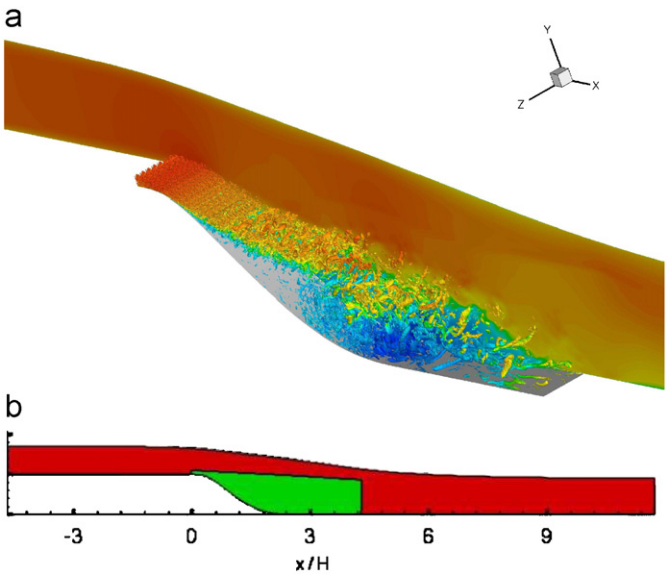

Fig. 21. Application of a database technique for the generation of fluctuations at an RANS/LES boundary; simulation of an air intake (courtesy of I. Mary, ONERA, Châtillon). (a) Instantaneous contours of Q; (b) setup of embedded LES: 2D RANS zone (red) and 3D LES zone (green).

5.2.1. Enrichment

Quéméré and Sagaut [49] developed a strategy called enrichment to allow for unsteady fluctuations to leave the LES domain. This technique scales fluctuations from inside the LES domain and adds these to mean values obtained from the RANS domain. The mean flow is directly coupled. The so-formed total flow quantity is copied to ghost cells at the LES-outflow boundary. A calibration constant is needed to determine the amount of scaling for the fluctuations. A modified version of enrichment was used at the downstream end of the air intake simulation shown in Fig. 21.

Enrichment has been fairly successful for compressible flows where pressure coupling needs not to be considered. There is some sensitivity to the grid stretching at the boundary and the numerical method employed. The calibration constant must be close to but in most cases smaller than 1. Otherwise, the method will cause reflections or the solution diverges. These shortcomings can be explained in the framework of the method discussed in Section 5.2.3 [112].

5.2.2. Using a controller in an overlap zone

Coupling of incompressible LES with compressible RANS was performed by Schlüter et al. [113]. At the inlet of an overlapping RANS domain, they prescribed the time and spatial averaged velocities and the resolved kinetic energy of the fluctuations from a specified plane inside the LES domain. The mean velocity field of the LES in the overlap region was driven toward the RANS target values using a simple controller and volume forces in the momentum equations. A convective condition was employed for the velocities at the outflow boundary of the LES. The pressure was determined by the solution of the pressure Poisson equation.

The method of Schlüter et al. has two main ingredients: a standard convective outflow condition for LES to minimize reflections and the coupling of the RANS flow field through a

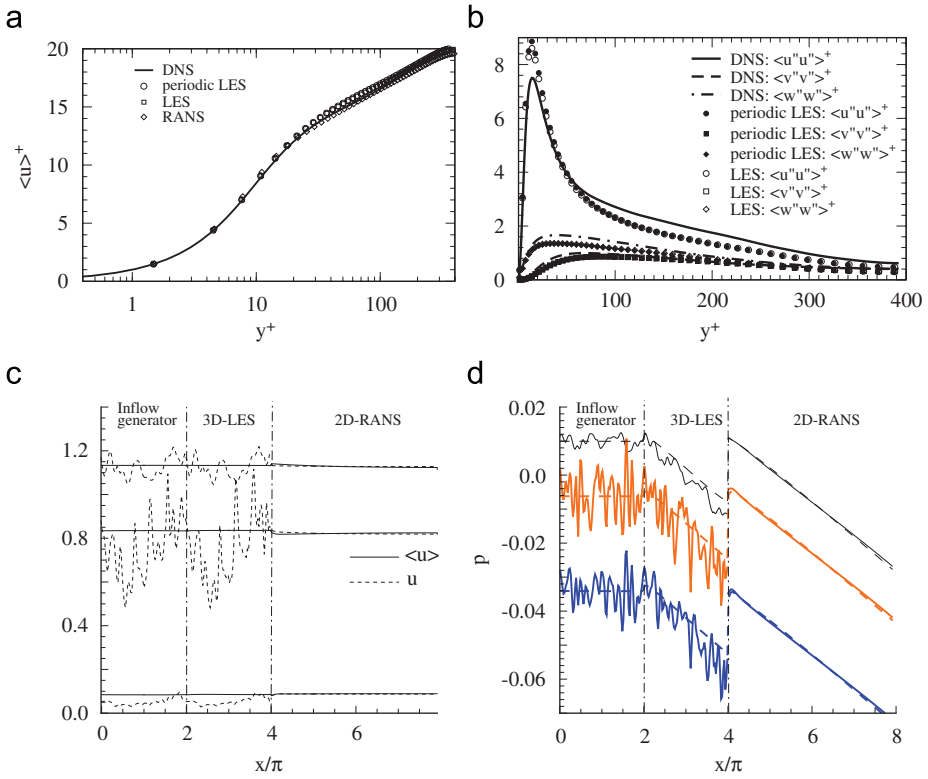

Fig. 22. RANS downstream of an LES zone with method P3 of [115] for turbulent channel flow at $Re_\tau = 395$. Top plots: profiles in near-wall scaling of (a) mean streamwise velocity and (b) normal components of the Reynolds stress tensor at the interface; DNS and periodic LES data for reference. Bottom plots: instantaneous and mean (c) velocities and (d) pressure for $y = 1$, 0.1 and 0.0037 (from top to bottom); pressure with arbitrary offset for clarity.

volume force field. This force essentially functions as a weak one-way upstream pressure coupling. Calibration of two constants is required: the length of the overlap region and a constant in the controller algorithm. Due to the overlap, this approach blurs the interface.

5.2.3. Convective velocity coupling

A general method for downstream coupling with a sharp interface was devised by von Terzi and Fröhlich [114,115]. For the velocity coupling, the explicitly Reynolds-averaged velocity field of the LES domain was imposed as a Dirichlet condition for the RANS inflow boundary. For the LES-outflow boundary, a discrete analog of a convective condition was prescribed for the velocity perturbation. This proposed velocity coupling is general and contains the enrichment strategy [49] as the limiting case of an infinite convection speed of the fluctuations [115]. No constant needs to be calibrated, since the local mean velocity at the interface can be used as the convection velocity for the fluctuations. A comparison of enrichment with the convective coupling can be found in [112].

For incompressible flows, the pressure coupling needs to be consistent with the elliptic nature of the Poisson equation but also with the chosen velocity coupling [115]. Furthermore, the pressure variable in incompressible solvers is often modified by the trace of model terms. If the model switches from LES to RANS, this changes the level of the pressure variable accordingly. This situation can be dealt with by completely decoupling the pressure between the subdomains, as if they were independent, and only coupling the velocities. As a consequence global mass conservation across the interface needs to be enforced explicitly so that the pressure solver converges in the subdomains [114].

5.2.4. Sample applications

The performance of different variations proposed in [115] were scrutinized for turbulent channel flow ($Re_\tau = 395$) by comparison with DNS data from [116]. This flow is fully developed so that any modification in the streamwise direction results from changes in modeling. Fig. 22a and b show statistical data in the wall-normal direction for the reference LES, for an LES without RANS coupling and at the interface plane for the hybrid method. The two lower plots of the figure illustrate that indeed instantaneous velocity and pressure fluctuations can leave the domain without reflections.

The channel flow is a sensitive but uncritical test case, as the flow is developed and therefore no downstream information is really needed for the upstream LES. This is different in the flow over periodic hills. For this case, the simulation is again divided into the three distinct zones used for the channel flow simulation (Fig. 23). The first zone is computed with LES using wall functions and periodic boundary conditions in the downstream direction serving as inflow generator for the second zone. $200 \times 64 \times 92$ interior cells were employed in the downstream, wall-normal and lateral direction, respectively. For the second zone, also LES was performed using the same resolution and wall-function as in zone 1, however, before the crest of the next hill is reached, the simulation switches from LES to RANS. At the outflow of the RANS domain, Neumann boundary conditions were applied. The position of the LES-to-RANS interface is challenging, but were selected on purpose for this test. Indeed, a simulation without the RANS zone using a standard convective outflow condition fails.

Typical results are displayed in Fig. 23. The instantaneous streamwise velocity contours show that the RANS flow field is completely steady. No reflections can be seen in the LES domain.

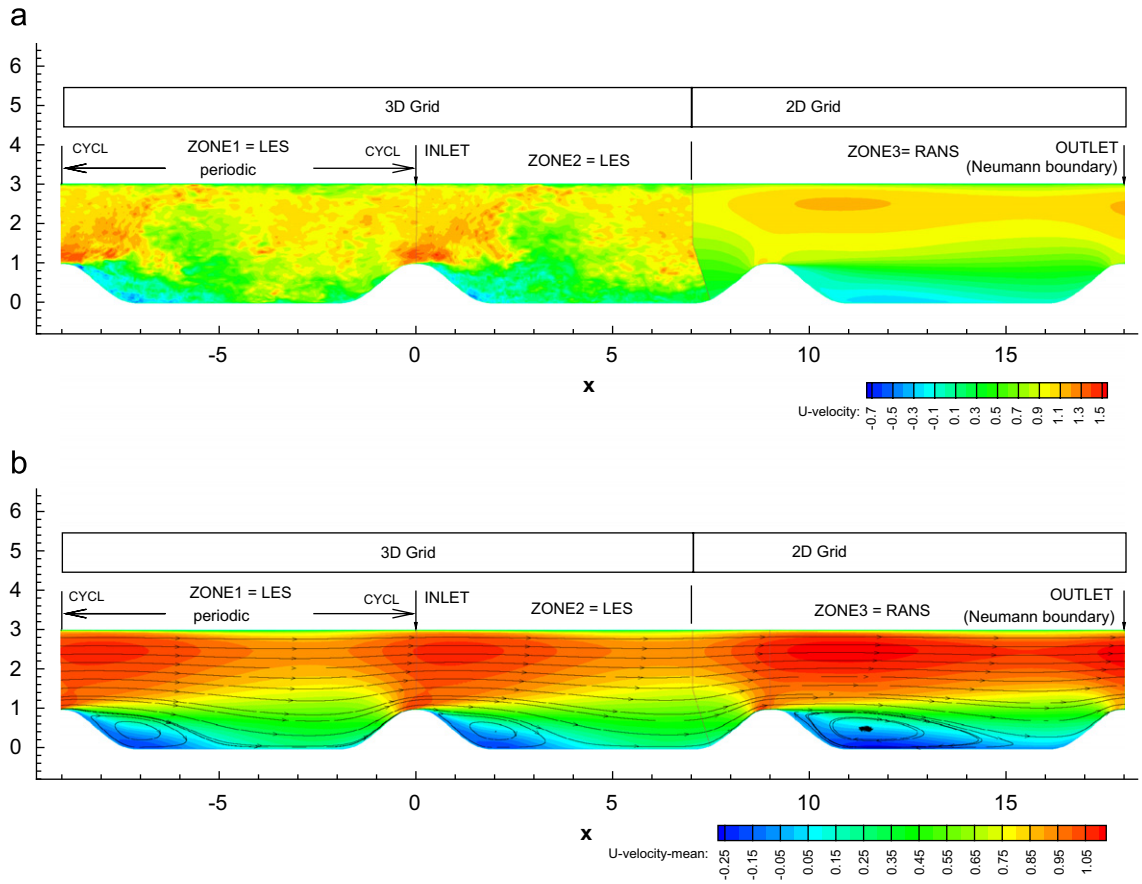

Fig. 23. Convective outflow coupling for the flow over periodic hills with the LES-to-RANS interface at $x \approx 7$ [114]. (a) Instantaneous streamwise velocity; (b) mean streamwise velocity.

The mean streamlines reveal that for the two-dimensional RANS solution reattachment occurs far too late, consistent with RANS results in the literature [4]. On the other hand, the LES in zone 2 delivers results similar to the reference solution of zone 1, albeit with a slightly longer recirculation region. Both reattachment lengths of 4.1 h and 4.3 h for zones 1 and 2, respectively, are acceptably close to the reference values of 4.6–4.7 h in [79] obtained with a substantially finer grid.

5.3. Tangential coupling

Subdomain boundaries more or less aligned with streamlines of the mean flow are called *tangential interfaces*. If these interfaces are close to walls with the RANS region between the LES domain and the wall, the problem is analogous to near-wall modeling of LES using the two-layer approach for unified modeling Section 4.2. With segregated modeling, however, the solution itself is coupled, i.e. the averaged and resolved velocity fields of the RANS and LES zones, respectively. Hence, the velocities are discontinuous over the interface, since only mean values are coupled. Fluctuations need to be provided separately. Tangential coupling with segregated modeling has so far been proposed only in [49] using the enrichment strategy discussed in Section 5.2.1. In this reference, the method was applied to turbulent channel flow and the flow over a bluff body.

5.4. Assessment

With a segregated approach, turbulence models are operated under conditions they were intended for. This avoids issues like lack of scale separation, gray zones and MSD, or double accounting as encountered for many other examples. On the other hand, segregated modeling requires the user to define *a priori* where LES and where RANS is to be performed. In particular for incompressible flows, coupling conditions at the interfaces have to be designed carefully due to the global nature of pressure in order not to spoil the simulation. The development of smart interfaces is challenging and not completed in the literature.

6. Second generation URANS models

RANS models are models only involving physical length-scales. LES models, in contrast, have been classified above as models containing, explicitly or implicitly, a length scale related to the numerical grid. This length scale determines the size of resolved fluctuations. Very recently, models have emerged which aim at resolving a substantial part of the turbulent fluctuations but do not contain such an explicit dependency on the computational grid. Consequently, we term these models *second generation URANS models* (2G-URANS). The essential characteristics, additional to the independence from the grid scale, is that the model contains a term sensing the amount of resolved fluctuations (temporal or spatial). This is in contrast to the classical URANS procedure described in Section 2.1.

6.1. The PANS model

6.1.1. Description of the method

The partially filtered Navier–Stokes (PANS) model[3] proposed by Girimaji [117], follows the idea put forth in Section 3.1 that unified models can be derived from existing RANS models by the introduction of some damping of model terms. The purpose of the damping is to adjust the given RANS model to better cope with situations where part of the turbulence is resolved. In contrast to the methods discussed in Section 3.1, no explicit damping function is devised here. Instead, for each characteristic scale of the turbulence closure, a constant damping ratio is prescribed prior to a given simulation. For the K–ε model this reads

$$f_K = \frac{K_\tau}{K} \quad \text{and} \quad f_\varepsilon = \frac{\varepsilon_\tau}{\varepsilon} \quad \text{with } 0 \leqslant f_K \leqslant f_\varepsilon \leqslant 1, \tag{41}$$

where K_τ and ε_τ represent the amount of unresolved kinetic energy and dissipation rate, respectively. In other words, the user decides *a priori* how much of the kinetic energy and dissipation rate is to be modeled. Note that the same ratio is then enforced everywhere in the flow field at any instant in time. The resulting scaling of ν_t in (10) becomes

$$\nu_t = C_{\mu\tau}\frac{K_\tau^2}{\varepsilon_\tau} = C_\mu \frac{f_K^2}{f_\varepsilon}\frac{K^2}{\varepsilon}, \tag{42}$$

where $C_{\mu\tau} = C_\mu$ was chosen by the author based on a fixed-point analysis of the RANS and PANS equations. The term f_K^2/f_ε constitutes the effective damping constant for the RANS model. For consistency, the transport equations of K and ε turn into equations for K_τ and ε_τ. These equations include the damping ratios, but also an additional term that requires modeling. With the specific models proposed in [117], the K_τ and ε_τ equations become formally identical to the original RANS closure. Only the model constants are replaced by parameters depending on f_K and f_ε.

6.1.2. Sample applications

So far only preliminary results have been published for turbulent flows in a lid driven cavity and over a cylinder. These are more of a qualitative nature and are hence not discussed here.

6.1.3. Assessment

A main advantage of the PANS model is its easy implementation into an existing RANS solver. Only coefficients need to be changed depending on the choices of f_K and f_ε. Furthermore, no explicit filtering is required, i.e. the filter is implied in the model and may actually vary in the computational domain since the velocity field is decomposed based on a desired amount of resolved kinetic energy rather than on a separation of scales using a filter with a certain width. Note, however, that numerical methods for standard RANS solvers are usually dissipative, particularly in time, whereas here temporal accuracy is desired depending on how much of the kinetic energy in the flow is to be resolved.

An important feature of the PANS approach is that it contains no explicit dependency on the grid-scale, i.e. it contains no elements qualifying as "LES" according to the definition in Section 2.4. Hence, it should be rather viewed as transforming an existing RANS model into a URANS model. The lack of this dependency, however, could be viewed as a drawback of the method for general applications: In hybrid LES/RANS methods, the user can choose a grid resolution deemed appropriate to resolve flow structures of interest in selected regions of the flow field. The SGS model then adjusts its level automatically based on the chosen local resolution. This is not possible here. The choice of f_K and f_ε defines a "constant resolution" everywhere in the flow field. Moreover, an appropriate choice to resolve a given large-scale flow feature of interest is not obvious, since energy and dissipation contents have to be prescribed and not spatial extent. In general, $f_\varepsilon \geqslant f_K$, since the dissipative scales are the smallest in a turbulent flow and are hence likely to require more modeling.

[3] This should not be confused with phase-averaged Navier–Stokes calculations occasionally also abbreviated as PANS.

For the URANS limit, $f_K < 1$ and $f_\varepsilon = 1$ and, for the LES limit, $f_K = f_\varepsilon \ll 1$ may be starting points for preliminary simulations.

Even though issues concerning wall-modeling, appropriate models for the additional terms in the transport equations for K_τ and ε_τ and, most of all, the specification of f_K and f_ε remain, the approach seems interesting, but requires substantially more testing.

6.2. Scale-adaptive simulation (SAS)

6.2.1. Description of the method

The scale-adaptive simulation (SAS) approach developed by Menter and co-workers resulted from revisiting the $K-KL$ model of Rotta [118] where K is the turbulent kinetic energy and L the traditional notation for the macro-length of turbulence. In [119], the idea is described considering the boundary-layer formulation of the model with the velocity gradient in the y-direction. The exact transport equation for KL then contains a sink term

$$-\frac{3}{16}\frac{\partial\langle u\rangle(\mathbf{x})}{\partial y}\int_{-\infty}^{\infty} R_{21}\,\mathrm{d}r_y - \frac{3}{16}\int_{-\infty}^{\infty}\frac{\partial\langle u\rangle(\mathbf{x}+\mathbf{e}_y r_y)}{\partial y}R_{12}\,\mathrm{d}r_y, \tag{43}$$

where $\mathbf{x}$ is a given point, r_y the distance, $\mathbf{e}_y$ the unit vector in the y-direction, and $R_{ij}(\mathbf{x},\mathbf{y}) = \langle u_i'(\mathbf{x}); u_i'(\mathbf{x}+\mathbf{y})\rangle$ the two-point correlation of the velocity fluctuations. A Taylor series of the second term in (43) yields

$$\frac{\partial\langle u\rangle}{\partial y}\int R_{12}\,\mathrm{d}r_y + \frac{\partial^2\langle u\rangle}{\partial y^2}\int R_{12}r_y\,\mathrm{d}r_y + \frac{1}{2}\frac{\partial^3\langle u\rangle}{\partial y^3}\int R_{12}r_y^2\,\mathrm{d}r_y + \cdots. \tag{44}$$

It is then natural to model the sum of the first term in (44) and the first term in (43) together as $\langle u'v'\rangle\tilde{\zeta}_1 L\partial\langle u\rangle/\partial y$, where $\tilde{\zeta}_1$ is a model constant. In isotropic turbulence, the two-point correlation R_{12} is symmetric w.r.t. $\mathbf{y}=0$. The integral of the second term in (44) hence vanishes in this case. For that reason, Rotta dropped this term for his model [118]. The third term on the other hand is non-zero and was modeled by Rotta as

$$\langle u'v'\rangle\tilde{\zeta}_2 L^3\frac{\partial^3\langle u\rangle}{\partial y^3}, \tag{45}$$

where $\tilde{\zeta}_2$ is a model constant. Since the third derivative is numerically delicate to evaluate and somewhat strange to use for modeling without retaining the second derivative, in actual implementations term (45) was never included. Under these conditions, however, the $K-KL$ model looses its particularity and becomes equivalent to other two-equation models.

Menter et al. [120] recognized that the integral of R_{12} is non-zero in non-homogeneous flows which, after all, constitute the area of application for the model. They proposed two models for this term:

$$\frac{3}{16}\frac{\partial^2\langle u\rangle}{\partial y^2}\int R_{12}r_y\,\mathrm{d}r_y \approx \zeta_2\langle u'v'\rangle\left|\frac{\partial^2\langle u\rangle}{\partial y^2}\right|L^2, \tag{46}$$

$$\frac{3}{16}\frac{\partial^2\langle u\rangle}{\partial y^2}\int R_{12}r_y\,\mathrm{d}r_y \approx \zeta_2\langle u'v'\rangle\left|\frac{\partial^2\langle u\rangle}{\partial y^2}\right|L^2\frac{1}{\kappa}\left|\frac{\partial L}{\partial y}\right|, \tag{47}$$

with κ being the von Kármán constant and ζ_2 a model parameter. These two choices were blended by replacing ζ_2 in (47) with

$$\hat{\zeta}_2 = \zeta_2\max\left\{C_{\mathrm{SAS}};\frac{1}{\kappa}\left|\frac{\partial L}{\partial y}\right|\right\}. \tag{48}$$

In [119], using transport equations for K and $\Phi=\sqrt{K}L$, the authors showed that the term proportional to the second derivative introduces another length-scale in addition to L, the von Kármán length-scale

$$L_{\mathrm{vk}} = \kappa\left|\frac{\partial U/\partial y}{\partial^2 U/\partial y^2}\right|. \tag{49}$$

The computed length-scale $L=\Phi/\sqrt{K}$ then differs according to which of the terms in (48) is larger. If C_{SAS} is smaller than the other contribution, L is proportional to $\sqrt{\delta L_{\mathrm{vK}}}$, where δ is the thickness of the shear layer. In the other case, L is proportional to L_{vK}. This was demonstrated by considering the artificial flow field $\langle u\rangle = U_0\sin(2\pi y/\lambda)$, $v=w=0$ as depicted in Fig. 24a and imposing $K=\Phi=0$ on the boundaries. Two cases were considered, one with the domain $y=0\ldots4\lambda$, the other with $y=0\ldots8\lambda$. The right plot in this figure shows the computed length scale L as a function of y. If $C_{\mathrm{SAS}}=0$, L scales with the square root of δ, which is $\delta=4\lambda$ in one case and $\delta=8\lambda$ in the other case. With $C_{\mathrm{SAS}}=0.54$ (obtained by calibration with unsteady isotropic turbulence) the length scale is substantially smaller and independent of the layer thickness, i.e. dependent only on L_{vK}. Fig. 24 illustrates the reduction of the turbulent length-scale, and hence the eddy viscosity, through the additional second-derivative term. It was found that in practical computations the limiting in (48) is not needed for the model to switch to its unsteady mode, since in that case the $|\partial L/\partial y|$-term turned out to be smaller than C_{SAS}. This switch hence was dropped in the variant of the model used to date [121] effectively resulting in a reduction of the coefficient ζ_2 to attain the desired capability of the model.

So far the notation $\langle u_i\rangle$ was used in the equations to indicate the statistical average and K, L, etc. were assumed to be statistical quantities. The purpose of the SAS model, however, is to be run in unsteady mode when appropriate. In that case, all variables are fluctuating instantaneous quantities resolving a sizable part of the total turbulent motion. It is hence suitable to reflect this by the notation. In the following, variables without brackets are used defining

$$U_i = \begin{cases}\langle u_i\rangle & \text{if the model runs in steady mode,}\\ \overline{u}_i & \text{if the model runs in unsteady mode}\end{cases} \tag{50}$$

and similarly for all other quantities.

The next step is to generalize the model for arbitrary directions of shear. Working with $\Phi=\sqrt{K}L$ instead of KL used in the Rotta model is convenient since this quantity corresponds to

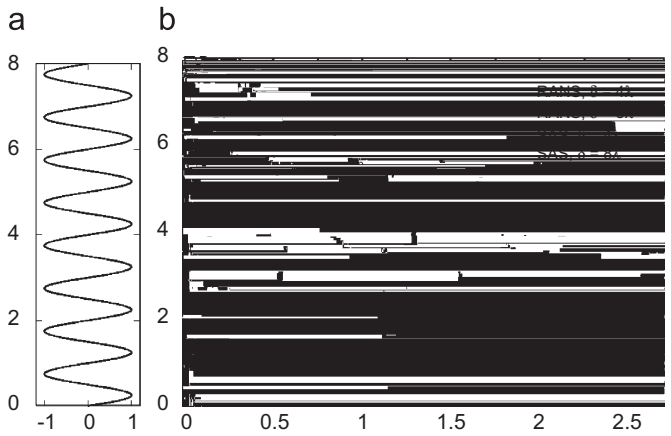

Fig. 24. Illustration of the RANS-mode and the SAS-mode of the SAS approach. (a) Model solution as discussed in the text. (b) Resulting length scale L, normalized with the period length λ. In the case of $\delta=4\lambda$, the velocity is unchanged but the computational domain extends only to half the height. The right figure is reproduced from [119]. (a) $U(y)$; (b) y/λ over L/λ.

the eddy viscosity via

$$\nu_t = \frac{\mu_t}{\rho} = c_\mu^{1/4}\Phi. \tag{51}$$

This results in the following model transport equations, written in the most current form in use to date [122]:

$$\frac{\partial(\rho K)}{\partial t} + \frac{\partial(\rho U_j K)}{\partial x_j} = P_K - c_\mu^{3/4}\rho\frac{K^{3/2}}{L} + \frac{\partial}{\partial x_j}\left(\frac{\mu_t}{\sigma_K}\frac{\partial K}{\partial x_j}\right), \tag{52}$$

$$\frac{\partial(\rho\Phi)}{\partial t} + \frac{\partial(\rho U_j \Phi)}{\partial x_j} = \frac{\Phi}{K}P_K\left(\zeta_1 - \zeta_2\left(\frac{L}{L_{vK}}\right)^2\right) - \zeta_3\rho K + \frac{\partial}{\partial x_j}\left(\frac{\mu_t}{\sigma_\Phi}\frac{\partial\Phi}{\partial x_j}\right), \tag{53}$$

$$L_{vK} = \kappa\frac{|U'|}{|U''|}, \quad |U'| = \sqrt{\frac{\partial U_i}{\partial x_j}\frac{\partial U_i}{\partial x_j}}, \quad |U''| = \sqrt{\frac{\partial^2 U_i}{\partial x_j \partial x_j}\frac{\partial^2 U_i}{\partial x_k \partial x_k}}, \tag{54}$$

$$P_K = \mu_t S^2, \quad S = \sqrt{2S_{ij}S_{ij}}, \quad S_{ij} = \frac{1}{2}\left(\frac{\partial U_i}{\partial x_j} + \frac{\partial U_j}{\partial x_i}\right). \tag{55}$$

The values of the constants are $c_\mu = 0.09$, $\kappa = 0.41$, $\zeta_1 = 0.8$, $\zeta_2 = 1.47$, $\zeta_3 = 0.0288$, $\sigma_K = \sigma_\Phi = 2/3$. The model is now able to switch from the steady RANS mode to an unsteady SAS mode where the computed length-scale is reduced yielding a lower eddy viscosity which in turn allows fluctuations to arise and to be sustained.

The above model was also converted into a modification of the widely used SST model proposed in [62]. The SAS approach is then rephrased as an additional source term in the ω-equation with some minor changes in order to preserve the RANS behavior of the SST model for boundary layer flows [123]. The most current version of this source term then reads [121]:

$$F_{SAS} = \max\left\{\rho\zeta_2\kappa S^2\left(\frac{L}{L_{vK}}\right)^2 - C\frac{2\rho K}{\sigma_\Phi}\max\left[\frac{1}{\omega^2}\frac{\partial\omega}{\partial x_j}\frac{\partial\omega}{\partial x_j}; \frac{1}{K^2}\frac{\partial K}{\partial x_j}\frac{\partial K}{\partial x_j}\right]; 0\right\} \tag{56}$$

with $\zeta_2 = 3.51$ and $C = 2$. Different numerical schemes are used in both modes as proposed for DES by Strelets [72]: an upwind scheme in RANS mode for stability reasons and second-order accurate central differences in SAS mode to avoid numerical damping.

So far, the model does not contain any parameter related to the grid used for solving the transport equations. Instead, a second physical length-scale is introduced to reduce the eddy viscosity. This is why the approach is a 2G-URANS model. In the unstable mode, the method is able to produce reasonable spectra for isotropic turbulence [119]. The way this takes place, however, is fairly intricate since several terms in the equations interact, further complicated by the switch in the numerical scheme.

While the model, in principle, can switch to an unsteady mode, it is understood that fluctuations in the SAS mode can only be sustained for frequencies that are sufficiently resolved by the computational grid and the time discretization. It was hence advocated that near the cutoff wavenumber of the grid some mechanism should be introduced which damps the fluctuations near the cutoff frequency [124]. Such a mechanism introduces a lower bound for the eddy viscosity ensuring that it does not drop below levels an SGS model would yield. This, however, requires the step size of the grid to appear, either explicitly via a true SGS model, or implicitly by numerical diffusion (like MILES for LES [44]). In other words, an LES component is incorporated into the model, but it is not the dominant characteristic of the approach. Furthermore, in the limit of vanishing step size the method does not revert to DNS. It still provides an eddy viscosity and merely becomes a highly resolved SAS. Further variants of the SAS model were proposed in the sequel, such as a one-equation variant, solving only an equation for $\Phi = \sqrt{K}L$ and replacing the transport equation for K by the algebraic expression $\nu_t S/\sqrt{c_\mu} = c_\mu^{-1/4} S\Phi$ [122].

To conclude this section, the definition of SAS is provided to distinguish the approach from other methods. Rephrased after [124] it reads:

1. The model contains two length scales, the classical one related to the first derivative of the resolved velocity, and a second one related to higher derivatives of the resolved velocity.
2. (a) The model provides RANS performance in stable flow regions (without explicit grid or time-step dependency).
   (b) The model allows the break-up of large unsteady structures into a turbulent spectrum (without explicit grid or time-step dependency).
   (c) The model provides proper damping of resolved turbulence at the resolution limit of the grid. This requires some information about the step size of the grid, either explicitly or implicitly.

6.2.2. Sample applications and assessment

Menter and co-workers applied the SAS model and variants to several configurations ranging from isotropic turbulence for calibration [119] to turbulent flows with heat transfer [122] and reactive flows [124]. They also computed the flow over periodic hills discussed above using roughly 2.5 million cells. Observe that with this amount of grid points standard LES can yield very reasonable results [80]. Fig. 25 shows profiles of the mean streamwise velocity and the turbulent kinetic energy for two different sizes of the time step, $\Delta_t = 0.05U_b/h$ and $0.2U_b/h$, where U_b is the bulk velocity over the crest of the hills. Both simulations exhibit good agreement in the velocity profiles compared to the reference LES, but for K the simulation with a larger time step deviates from the reference data.

In Fig. 26, a vortex identification criterion is used to demonstrate that SAS can indeed resolve unsteady flow structures, but again the temporal resolution has a marked impact on the results. That this is beyond a mere increase in artificial damping due to the numerical method is corroborated by the coloring of the contours as a measure for the ratio of turbulent to molecular viscosity. An increase for the coarse resolution can be discerned that is in contrast to how a traditional LES would react to insufficient temporal resolution. For LES, an increase in temporal damping by large time steps would decrease resolved flow gradients but also incur a concomitant decrease of the SGS viscosity. For SAS, however, the increase in smoothness of the solution leads to larger values of the eddy viscosity equivalence Φ. The mechanism for this can be found in (53). Since a smoother resolved velocity field yields a larger von Kármán length scale, the ratio of L over L_{vK} decreases and hence the production of Φ increases. On the other hand a smoother resolved velocity field also decreases the production of K in (55) which feeds back on the production and dissipation of Φ in intricate ways. The resulting net increase of the eddy viscosity can drive SAS to its steady mode in case of coarse resolution. This can be seen as a safeguard in simulations of complex flows, but it also bears difficulties and may incur higher resolution requirements than other hybrid methods in order to obtain unsteady results. An indication for the latter will be discussed in the following:

Kniesner et al. [90] converted the model into a K–ε variant and computed also the flow over periodic hills, but on a coarser grid of only 500,000 cells, almost an order of magnitude less than the reference LES in [79]. The results with their version of SAS

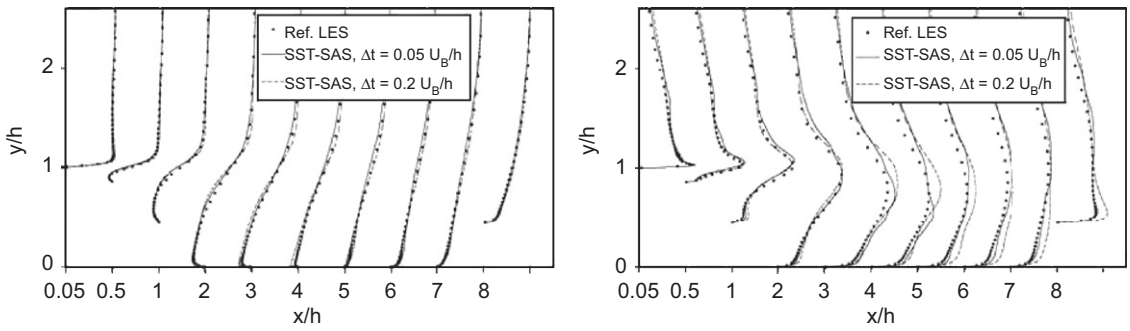

Fig. 25. Statistical data from SAS simulations of the flow over periodic hills performed with two time steps, $\Delta_t = 0.05U_b/h$ and $0.2U_b/h$ corresponding to the graphs in Fig. 26. Left: Profiles of mean streamwise velocity. Right: Sum of modeled and resolved turbulent kinetic energy (courtesy of F.R. Menter, 2008).

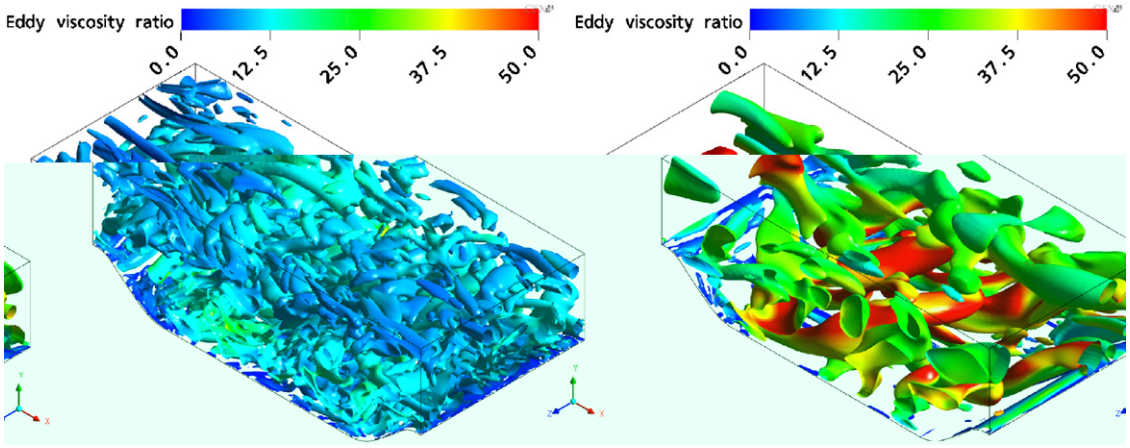

Fig. 26. SAS applied to the flow over periodic hills. Iso-surface of the vortex identification criterion $Q = (\Omega^2 - S^2)/2$, colored by the ratio of the eddy viscosity to the molecular viscosity. Two different time steps were used: left: $\Delta_t = 0.05U_b/h$, right: $\Delta_t = 0.2U_b/h$ (courtesy of F.R. Menter, 2008).

concerning the mean profile and the resolved turbulent kinetic energy, however, were not as good as those obtained with the interfacing hybrid method proposed in the same paper [90]. Davidson [125] used SAS to compute the developing flow in a channel, the flow in an asymmetric diffusor and the flow over a three-dimensional hill comparing the results to SST–URANS simulations of the same flow. For the diffusor the model did not run in any of the two limits—SAS or RANS—but somewhere in between, yielding poorer results than SST–URANS. The hill flow was poorly predicted by both options, while hybrid LES/RANS of the same author [126] performed better. From such examples and the channel flow simulations in the original SAS proposal [120], it seems that, for flows where traditional URANS methods yield steady flow predictions, the driving force pushing SAS to its unsteady mode is missing. This may well be due to the mechanism for increasing Φ described above. Hence, such cases constitute a severe challenge for SAS and the method should not be applied when flow instabilities are weak.

Since the SAS method is very young it is too early to definitively conclude about its capacities. Its big advantage is the simplicity with which it can be implemented into an existing RANS solver, i.e. the insertion of a single additional term into a model transport equation, such as (56). Furthermore, the user is not requested to specify model parameters or to control them through the choice of the computational grid which is an immense advantage in case of industrial applications. The switch from the steady to the unsteady mode is triggered by the model itself and is not sufficiently understood yet. For resolutions too coarse to resolve the fluctuations the method tends to switch to a steady RANS solution. The resolution requirements of SAS certainly depend on the respective case to which the method is applied and the desired type of results. As with other methods, under-resolution in intermediate regimes bears uncertainty. Comparison of effort and performance of SAS w.r.t. other hybrid methods remains to be quantified.

6.3. Layering 2G-URANS and LES

6.3.1. Description of the method

Medic et al. [127] proposed a near-wall model for LES of attached flows which aims at avoiding the MSD addressed in Section 3.2.3. Starting from a RANS model, the idea is to subtract from this model the turbulent stresses or the equivalent model contribution that is already accounted for by the resolved fluctuations. This was performed for an eddy-viscosity model leading to

$$\begin{aligned} \nu_t^{\text{blended}} &= \nu_t^{\text{RANS}} - \nu_t^{\text{resolved}} \\ &= \nu_t^{\text{RANS}} + \langle \overline{u}'\overline{v}' \rangle \Big/ \frac{\partial \langle \overline{u} \rangle}{\partial y}, \end{aligned} \tag{57}$$

where $\langle \cdots \rangle$ represents an explicit average of the computed solution in directions of homogeneous statistics and/or in time, while $\overline{u}$ and $\overline{v}$ are the resolved streamwise and wall-normal velocities, respectively. Eq. (57) is used instead of ν_t^{LES} for y^+, based on the average flow, below a specified value, e.g. $(y^+)^* = 50$, while for larger distances, the unmodified LES model ν_t^{LES} is employed. This constitutes a hard interface between layered 2G-URANS and

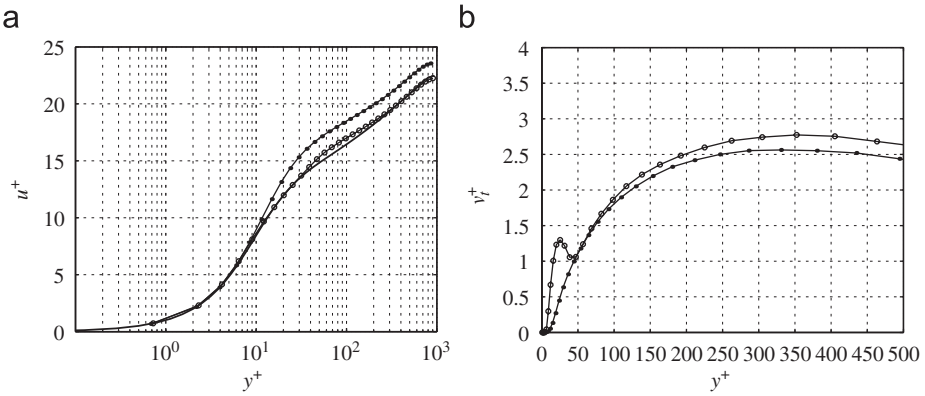

Fig. 27. Turbulent channel flow at $Re_\tau = 950$ using a RANS-modified LES for $y^+ \leqslant 50$; — reference DNS, – ∘ – RANS-modified LES, – • – pure LES. Figures reproduced from [127]. (a) Mean streamwise velocity; (b) eddy viscosity.

LES. In addition to (57) the resulting eddy viscosity is clipped at the (instantaneous) value obtained from the SGS-model:

$$\nu_t = \max\{\nu_t^{\text{blended}}; \nu_t^{\text{LES}}\}. \tag{58}$$

This results in a blending between the LES and RANS limits since

$$\nu_t^{\text{LES}} \leqslant \nu_t \leqslant \nu_t^{\text{RANS}} \tag{59}$$

or, equivalently,

$$0 \leqslant \frac{\nu_t^{\text{LES}}}{\nu_t^{\text{RANS}}} \leqslant \frac{\nu_t}{\nu_t^{\text{RANS}}} \leqslant 1, \tag{60}$$

with the ratio $\nu_t/\nu_t^{\text{RANS}}$ being a measure of the amount of blending. This factor approaches one if only little of the turbulent stresses is resolved, whereas the model switches itself off if the simulation is well resolved. As RANS closures, the K–ω model and the Spalart–Allmaras model were tested, while the wall-adapted local eddy viscosity (WALE) model or the dynamic Smagorinsky model were used as SGS models. Other variants are easily conceived.

For very simple flows, ν_t^{RANS} can be obtained via a database such that the hybrid method reduces to a one-way coupling similar to a wall function. For more complex flows, the RANS solution is to be computed together with the LES in a coupled fashion: the resolved velocity is explicitly averaged to provide the mean velocities and strain rates in the convective and production terms of the transport equations employed in the RANS model which in turn is used to determine ν_t^{RANS}. In contrast to other hybrid models, like DES, the RANS model term is obtained from the averaged, not the instantaneous solution. This reduces the eddy viscosity as the gradients of the instantaneous solution are larger.

The model according to (57) is a RANS-type model as it does not involve the grid scale. In fact, it is a 2G-URANS model as it accounts for the resolved fluctuations when run in unsteady mode. If no fluctuations are introduced, the solution is steady and equal to the classical RANS solution. If fluctuations are present they reduce the eddy viscosity and hence the damping so that unsteadiness is enhanced compared to the traditional URANS approach described in Section 2.1.

6.3.2. First applications

Preliminary results for turbulent channel flow at $Re_\tau = 395$ and 950 were presented in [127,128]. Compared to an unsteady simulation employing ν_t^{RANS}, the blended model (57) yields increased resolved fluctuations.

Fig. 27 reports mean values from a computation at the higher Reynolds number using the full algorithm. LES and a K–ω-based RANS calculation were performed in a coupled fashion up to $(y^+)^* = 50$. The figure shows the improvement of the RANS-modified LES compared to a pure LES using the WALE subgrid-scale model, a model accounting for the reduction of the eddy viscosity near the wall without the need of van Driest damping. Part (b) of the figure illustrates the increase in ν_t generated by the blending with the RANS viscosity. The Reynolds stresses (not reproduced here) only exhibit a sizable difference in $\langle \overline{u}'\overline{u}' \rangle$ of which the overshoot w.r.t. the DNS data are somewhat reduced.

6.3.3. Assessment

A drawback of the method is the need for explicit averaging to determine the correction term in (57). It was performed in homogeneous directions in the calculation discussed above, but could also be replaced by averaging in time. On the other hand, the approach avoids double accounting for fluctuations by subtracting the resolved motion. Computations of channel flow with the coupled model were also undertaken in collaboration with the present authors by Brandt and Hellsten [129] using the $K-\omega$ RANS model and the Smagorinsky SGS model. In these simulations, substantial sensitivity of the result w.r.t. details of the simulation was observed (SGS model constant, position of interface, averaging procedure). It was demonstrated that the steep gradient in ν_t around y^* introduced by the blending yields a jump in $\mathrm{d}\langle\overline{u}\rangle/\mathrm{d}y$ which in turn influences the production term of the underlying RANS model. Simulations of the periodic hill configuration showed less sensitivity due to the more complex nature of the flow. Further studies are clearly needed for a final assessment of this approach.

7. Concluding remarks

In the previous sections, a large number of methods was discussed combining LES and RANS features. The presentation was guided by the classification proposed in Section 2 which is based on distinguishing *segregated models* from *unified models* and *interfacing* from *blending* for deriving the latter. According to their variability in time, interfaces were furthermore classified as either *soft* or *hard*. Finally, the term *2G-URANS* models was introduced to emphasize the difference of SAS and PANS from traditional *URANS* models, but also to separate them from *LES* or the hybrid LES/RANS techniques discussed before. Together with the traditional approaches URANS, LES and DNS, these methods constitute

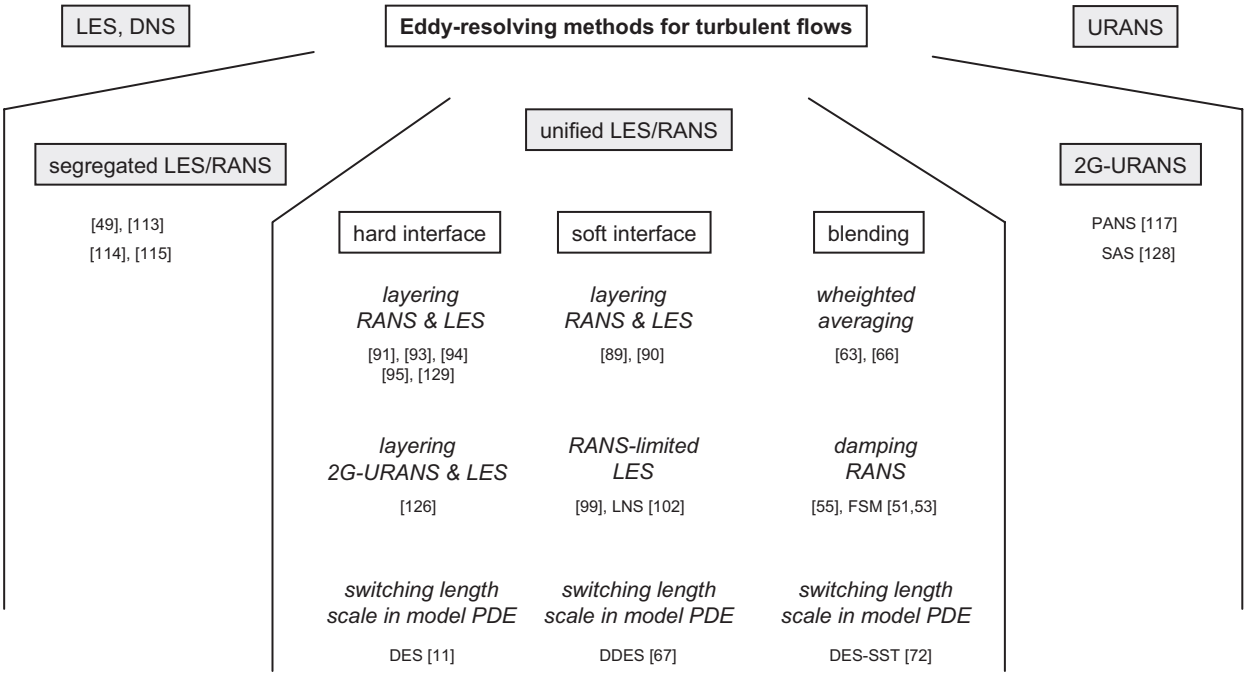

Fig. 28. Classification scheme developed in the present paper covering traditional and recent approaches to eddy-resolving simulations of turbulent flows. Key references of methods discussed are repeated here with common acronyms added where available. It is understood that many more references could be added which is not possible here for lack of space.

eddy-resolving approaches to the simulation of turbulent flows. The full picture, with the classification scheme proposed here, is visualized in Fig. 28.

Throughout the discussion of the models, their respective features were commented, naming advantages and difficulties so that this is not reiterated here. Certain issues have been repeatedly addressed such as the difficulty of a continuous transition between LES and RANS. In this respect, the direction of transfer of turbulent kinetic energy in space within the flow is certainly an aspect to be taken into account.

Other issues could only be mentioned marginally here, such as the influence of the numerical discretization scheme, which may however be of considerable practical importance. In general, numerical methods optimized for the RANS limit are poor choices for DNS and vice versa. For classical LES, as for DNS, low-dissipation schemes are preferred, whereas for RANS numerical stability is paramount. In between, the choices and trade offs are considerably more difficult to make.

Finally, the issue of how actually to compare a computed hybrid LES/RANS solution to experimental data merits consideration. Generally, one has to add modeled and resolved contributions, although this may be delicate with certain models. The issue of grid refinement studies and convergence of models in the limit of vanishing grid size or in other limits could not be elaborated for lack of space here.

Hybrid LES/RANS methods, or other methods with a larger contribution of modeled turbulent fluctuations that are still able to resolve the largest unsteady flow structures, are a very active field of research. Extensive testing of the various approaches is needed to strengthen confidence in these methods and to delineate their respective range of applicability.

Acknowledgements

This research was funded by the German Research Foundation under FR 1593/1 and SFB 606. Computing time was provided by SCC Karlsruhe. The authors acknowledge valuable discussions with Wolfgang Rodi, Ivan Mary, Suad Jakirlić, Florian Menter, and Richard Sandberg.

References

[1] Casey M, Wintergerste T. Best practice guidelines. ERCOFTAC; 2000.
[2] Rodi W, Bonnin JC, Buchal T, editors. ERCOFTAC workshop on data bases and testing of calculation methods for turbulent flows. University of Karlsruhe, Germany; April 1995.
[3] Hellsten A, Rautaheimo P, editors. Proceedings of 8th ERCOFTAC/IAHR/COST workshop on refined turbulence modelling. Helsinki University of Technology; 1999.
[4] Jakirlić S, Jester-Zürker R, Tropea C, editors. 9th ERCOFTAC/IAHR/COST workshop on refined turbulence modelling, October 2–5, 2001, Darmstadt University of Technology; 2001.
[5] Manceau R, Bonnet JP. Proceedings of the 10th ERCOFTAC/IAHR/QNET-CFD workshop on refined turbulence modelling, Laboratoire d'études Aerodynamiques, UMR CNRS 6609, Université de Poitiers, France; 2003.
[6] Breuer M, Lakehal D, Rodi W. Flow around a surface mounted cubical obstacle: comparison of LES and RANS- results. In: Deville M, Gavrilakis S, Ryming IL, editors. Computation of 3D complex flows notes on numerical fluid mechanics, vol. 53. Braunschweig: Vieweg; 1996. p. 22–30.
[7] Hinterberger C, García-Villalba M, Rodi W. LES of flow around the Ahmed body. In: McCallen M, et al., editors. Aerodynamics of heavy vehicles: truck, busses and trains. Lecture notes in applied and computational mechanics, vol. 19. Berlin: Springer; 2004. p. 77–87.
[8] Ahmed SR, Ramm G. Some salient features of the time-averaged ground vehicle wake. SAE-Paper 840300, 1984.
[9] Lienhart H, Becker, S. Flow and turbulence structure in the wake of a simplified car model. SAE Paper 2003-01-0656; 2003.
[10] Chapman DR. Computational aerodynamics development and outlook. AIAA J 1979;17:1293–313.
[11] Spalart PR, Jou W-H, Strelets M, Allmaras SR. Comments on the feasibility of LES for wings, and on a hybrid RANS/LES approach. In: Liu C, Liu Z, editors. Advances in DNS/LES. Greyden Press; 1997.
[12] Deardorff JW. A numerical study of three-dimensional turbulent channel flow at large Reynolds numbers. J Fluid Mech 1970;41:453–80.
[13] Schumann U. Subgrid scale model for finite difference simulations of turbulent flows in plane channels and annuli. J Comput Phys 1975;18: 376–404.
[14] Werner H, Wengle H. Large-eddy simulation of turbulent flow over and around a cube in a plane channel. In: Durst F, Friedrich R, Launder BE, Schmidt FW, Schumann U, Whitelaw JH, editors. Selected papers from the 8th symposium on turbulent shear flows. Berlin: Springer; 1993. p. 155–68.

[15] Wang M, Moin P. Computation of trailing-edge flow and noise using large-eddy simulation. AIAA J 2000;38:2201–9.
[16] Wang M, Moin P. Dynamic wall modeling for large-eddy simulation of complex turbulent flows. Phys Fluids 2002;14:2043–51.
[17] Cabot W. Large eddy simulations with wall models, In: Annual research briefs—1995, Center for Turbulence Research, Stanford University; 1995.
[18] Balaras E, Benocci C, Piomelli U. Finite-difference computations of high Reynolds number flows using the dynamic subgrid-scale model. Theoret Comput Fluid Dyn 1995;7:207–16.
[19] Piomelli U, Chasnov JR. Large-eddy simulations: theory and applications. In: Hallbäck M, Henningson DS, Johansson AV, Alfredson PH, editors. Turbulence and transition modelling. Dordrecht: Kluwer Academic Publisher; 1996. p. 269–331.
[20] Sagaut P. Large eddy simulation of incompressible flows. 3rd ed. Berlin: Springer; 2006.
[21] Fröhlich J. Large eddy simulation turbulenter Strömungen. Stutgart: Teubner; 2006.
[22] Speziale CG. A review of Reynolds stress models for turbulent shear flows. Report 95-15. ICASE; March 1995.
[23] Pope SB. Turbulent flows. Cambridge: Cambridge University Press; 2000.
[24] Rodi W. On the simulation of turbulent flows past bluff bodies. J Wind Eng Ind Aerodyn 1993;46-47:3–9.
[25] Hussain AKMF. Coherent structures and turbulence. J Fluid Mech 1986; 173:303–56.
[26] Wienken W, Stiller J, Keller A. A method to predict cavitation inception using large-eddy simulation and its application to the flow past a square cylinder. J Fluids Eng 2006;128:316–25.
[27] Rodi W, Ferziger JH, Breuer M, Pourquié M. Status of large eddy simulation: results of a workshop. J Fluids Eng 1997;119:248–62.
[28] Durbin P. Separated flow computations with the $k-\varepsilon-\overline{v^2}$ model. AIAA J 1995;33:659–64.
[29] Schwarze R. Private communication; 2005.
[30] Leonard A. Energy cascade in large eddy simulations of turbulent fluid flows. Adv Geophys 1974;18A:237.
[31] Fröhlich J, Rodi W. Introduction to large-eddy simulation of turbulent flows. In: Launder B, Sandham N, editors. Closure strategies for turbulent and transitional flows. Cambridge: Cambridge University Press; 2002. p. 267–98 [chapter 8].
[32] Tennekes H, Lumley JL. A first course in turbulence. Cambridge, MA: MIT Press; 1972.
[33] Schumann U. Direct and large-eddy simulation of turbulence—summary of the state of the art. In: Introduction to turbulence modelling II, vol. 1993-02. VKI-lecture series, Brussels, Belgium; Von Kármán Institute for Fluid Dynamics; 1993.
[34] Spalart PR. Young person's guide to detached eddy simulation grids. Technical Report NASA/CR-2001-211032, NASA Langley Research Center; 2001.
[35] Scotti A, Meneveau C, Lilly DK. Generalized smagorinsky model for anisotropic grids. Phys Fluids A 1993;5(9):2208–306.
[36] Ferziger JH. Large eddy simulation. In: Gatski TB, Hussaini MY, Lumley JL, editors. Simulation and modelling of turbulent flows ICASE/LaRC series in computer science engineering. New York: Oxford University Press; 1996. p. 109–54.
[37] Drikakis D. Special issue: very large eddy simulation. Int J Numer Methods Fluids 2002;39(9):763–864.
[38] Meri A, Wengle H, Raddaoui M, Chauve P, Schiestel R. Large-eddy simulation of non-equilibrium inflow conditions and of the spatial development of a confined plane jet with co-flowing streams. In: Rodi W, Laurence D, editors. Engineering Turbulence Modelling and Experiments, vol. 4. Amsterdam: Elsevier; 1999. p. 197–206.
[39] Pourquié M, Moulinec C, van Dijk A. A numerical wind tunnel experiment. In: Friedrich R, Rodi W, editors. Advances in LES of complex flows. Fluid mechanics and its applications, vol. 65. Dordrecht: Kluwer Academic Publishers; 2002. p. 115–30.
[40] Mason PJ, Callen NS. On the magnitude of the subgrid-scale eddy coefficient in large-eddy simulations of turbulent channel flow. J Fluid Mech 1986;162: 439–62.
[41] Geurts BJ, Fröhlich J. A framework for predicting accuracy limitations in large-eddy simulations. Phys Fluids 2002;14:L41–4.
[42] Stolz S, Adams NA, Kleiser L. An approximate deconvolution procedure for large-eddy simulation. Phys Fluids 1999;11:1699–701.
[43] Stolz S, Schlatter P, Kleiser L. High-pass filtered eddy-viscosity models for large-eddy simulation of transitional and turbulent flows. Phys Fluids 2005;17:1–14.
[44] Boris JP, Grinstein FF, Oran ES, Kolbe RL. New insights into large eddy simulation. Fluid Dyn Res 1992;10:199.
[45] Adams N, Hickel S, Franz S. Implicit subgrid-scale modeling by adaptive deconvolution. J Comp Phys 2004;200:412–31.
[46] Sagaut P, Deck S, Terracol M. Multiscale and multiresolution approaches in turbulence. Imperial College Press; 2006.
[47] Deck S. Zonal-detached-eddy simulation of the flow around a high-lift configuration. AIAA J 2005;43(11):2372–84.
[48] Nolin G, Mary I, Ta-Phuoc L, Hinterberger C, Fröhlich J. Coupling from LES to RANS using eddy-viscosity models. In: Direct and Large-Eddy Simulation VI, Poitiers, September 12–14, 2005, vol. VI. Dordrecht: Kluwer Academic Publishers; 2005.
[49] Quéméré P, Sagaut P. Zonal multi-domain RANS/LES simulations of turbulent flows. Int J Numer Methods Fluids 2002;40:903–25.
[50] Speziale CG. Computing non-equilibrium turbulent flows with time-dependent RANS and VLES. In: 15th international conference on numerical methods in fluid dynamics, Monterey; 1996.
[51] Speziale CG. Turbulence modeling for time-dependent RANS and VLES: a review. AIAA J 1998;36(2):173–84.
[52] Zhang HL, Bachman C, Fasel HF. Application of a new methodology for simulations of complex turbulent flows. AIAA Paper 2000-2535; 2000.
[53] Fasel HF, Seidel J, Wernz S. A methodology for simulation of complex turbulent flows. J Fluids Eng 2002;124:933–42.
[54] Fasel HF, von Terzi DA, Sandberg RD. A methodology for simulating compressible turbulent flows. J Appl Mech 2006;73:405–12.
[55] Hussaini MY, Thangam S, Woodruff SL, Zhou Y. Development of a continuous model for simulation of turbulent flows. J Appl Mech 2006;73:441–8.
[56] von Terzi DA, Sandberg RD, Sivasubramanian J, Fasel HF. High-accuracy DNS and LES of high Reynolds number supersonic base flows and passive control of the near wake. In: DoD high performance computing modernization program: proceedings of the user group conference. New York: IEEE press; June 2005.
[57] Speziale CG. A combined large-eddy simulation and time-dependent RANS capability for high-speed compressible flows. J Sci Comput 1998;13(3): 253–74.
[58] Sandberg RD, Fasel HF. Investigation of supersonic wakes using conventional and hybrid turbulence models. AIAA J 2006;44(9):2071–83.
[59] Sivasubramanian J, Sandberg RD, von Terzi DA, Fasel HF. Numerical investigation of flow control mechanisms for drag reduction in supersonic base flows. AIAA Paper 2006–902; 2006.
[60] Sivasubramanian J, Sandberg RD, von Terzi DA, Fasel HF. Numerical investigation of transitional supersonic base flows with flow control. J Spacecr Rockets 2007;44(5):1021–8.
[61] Fröhlich J, Rodi W, Bertoglio JP, Bieder U, Touil M. Large eddy simulation of flow around circular cylinders on structured and unstructured grids, II. In: Hirschel EH, editor. Numerical flow simulation II. Notes on numerical fluid mechanics, vol. 75. London: Vieweg; 2001. p. 231–49.
[62] Menter FR. Two-equation eddy viscosity turbulence models for engineering applications. AIAA J 1994;32:1598–605.
[63] Fan TC, Tian M, Edwards JR, Hassan HA, Baurle RA. Validation of a hybrid Reynolds-averaged/large-eddy simulation method for simulating cavity flameholder configurations. AIAA Paper 2001–2929; 2001.
[64] Fan TC, Tian M, Edwards JR, Hassan HA, Baurle RA. Hybrid large-eddy/Reynolds-averaged Navier–Stokes simulations of shock-separated flows. J Spacecr Rockets 2004;41(6):897–906.
[65] Xiao X, Edwards JR, Hassan HA. Blending functions in hybrid large eddy/Reynolds-averaged Navier–Stokes simulations. AIAA J 2004;42(12): 2508–15.
[66] Baggett JS. On the feasibility of merging LES with RANS for the near-wall region of attached turbulent flows. In: Annual research briefs—1998. Center for Turbulence Research; 1998.
[67] Spalart PR, Deck S, Shur ML, Squires KD, Strelets MK, Travin A. A new version of detached-eddy simulation resistant to ambiguous grid densities. Theoret Comput Fluid Dyn 2006;20:181–95.
[68] Spalart PR, Allmaras SR. A one-equation turbulence model for aerodynamic flows. La Rech Aèrosp 1994;1:5–21.
[69] Shur M, Spalart PR, Strelets M, Travin A. Detached-eddy simulation of an airfoil at high angle of attack. In: Rodi W, Laurence D, editors. Engineering turbulence modelling and experiments, vol. 4. Amsterdam: Elsevier; 1999. p. 669–78.
[70] Spalart PR. The uses of DES: natural, extended, and improper. Invited lecture at DESider workshop, 14–15 July 2005, Stockholm, Sweden; 2005.
[71] Piomelli U, Balaras E, Pasinato H, Squires KD, Spalart PR. The inner-outer layer interface in large-eddy simulations with wall-layer models. Int J Heat Fluid Flow 2003;24:538–50.
[72] Strelets M. DES of massively separated flows. AIAA Paper 2001-0879; 2001.
[73] Hedges LS, Travin AK, Spalart PR. Detached-eddy simulations over a simplified landing gear. J Fluids Eng 2002;124:413–23.
[74] Forsythe JR, Squires KD, Wurtzler KE, Spalart PR. DES of fighter aircraft at high alpha. AIAA Paper 2002-0591; 2002.
[75] Squires KD, Forsythe JR, Morton SA, Blake DC, Serrano M, Wurtzler KE, et al. Analysis of full aircraft with massive separation using detached–eddy simulation. In: Proceedings of the high performance computing modernization programm 2002 users group conference, Austin, Texas; 2002.
[76] Spalart PR, Squires KD. The status of detached-eddy simulation for bluff bodies. In: Friedrich R, Métais O, editors. Direct and large eddy simulation V. Dordrecht: Kluwer Academic Publishers; 2004.
[77] Nikitin NV, Nicoud F, Wasisto B, Squires KD, Spalart PR. An approach to wall modelling in large-eddy simulations. Phys Fluids 2000;12:1629–32.
[78] Mellen CP, Fröhlich J, Rodi W. Large eddy simulation of the flow over periodic hills. In: Deville M, Owens R., editors. Proceedings of 16th IMACS world congress, pages CD–ROM, Lausanne, Switzerland; 2000.
[79] Fröhlich J, Mellen CP, Rodi W, Temmerman L, Leschziner MA. Highly-resolved large eddy simulations of separated flow in a channel with streamwise periodic constrictions. J Fluid Mech 2005;526:19–66.
[80] Šarić S, Jakirlić S, Breuer M, Jaffrézic B, Deng G, Chikhaoui O, et al. Evaluation of detached eddy simulations for predicting the flow over periodic hills. In: Proceedings of CEMRACS 2005, vol. 16. London: ESAIM; 2007. p. 133–45.

[81] Breuer M. New reference data for the hill flow test case. ⟨http://www.hy.bv.tum.de/DFG-CNRS/⟩; 2005.
[82] Temmerman L, Leschziner M, Mellen CP, Fröhlich J. Investigation of wall-function approximations and subgrid-scale models in large eddy simulation of separated flow in a channel with streamwise periodic constrictions. Int J Heat Fluid Flow 2003;24(2):157–80.
[83] Cokljat D, Liu F. DES of turbulent flow over an airfoil at high incidence. AIAA Paper 2002–0590, In: 40th aerospace sciences meeting and exhibit, 14–17 January 2002, Reno Nevada; 2002.
[84] Mellen CP, Fröhlich J, Rodi W. Lessons from the European LESFOIL project on LES of flow around an airfoil. AIAA Paper 2001-0111; 2001.
[85] Davidson L, Cokljat D, Fröhlich J, Leschziner MA, Mellen C, Rodi W., editors. LESFOIL: large eddy simulation of flow around a high lift airfoil. In: Notes on numerical fluid mechanics. vol. 83. Berlin: Springer; 2003.
[86] Schmidt S, Thiele F. Detached eddy simulation of airfoil flow on semi-structured grids. In: Friedrich R, Rodi W, editors. Advances in LES of complex flows. Dordrecht: Kluwer Academic Publishers; 2002. p. 255–72.
[87] Fröhlich J, Rodi W, Kessler Ph, Parpais S, Bertoglio JP, Laurence D. Large eddy simulation of flow around circular cylinders on structured and unstructured grids. In: Hirschel EH, editor. Numerical flow simulation. I. Notes on numerical fluid mechanics, vol. 66. Vieweg; 1998. p. 319–38.
[88] Fröhlich J, Mellen CP. Transition in LES of bluff body flows and airfoils. In: Geurts BJ, Friedrich R, Metais O, editors. Direct and large-eddy simulation, vol. IV. Dordrecht: Kluwer Academic Publishers; 2001. p. 145–56.
[89] Breuer M, Jaffrézic B. An advanced hybrid LES-RANS method. ERCOFTAC Bull 2007;72:41–4 (see also Breuer M, Jaffrézic B, Arora K. Hybrid LES–RANS technique based on a one-equation near-wall model, Theoret Comput Fluid Dyn 2007).
[90] Kniesner B, Šarić S, Mehdizadeh A, Jakirlić S, Hanjalić K, Tropea C, et al. Wall treatment in LES by RANS models: method development and application to aerodynamic flows and swirl combustors. ERCOFTAC Bull 2007;72:33–40.
[91] Cabot W, Moin P. Approximate wall boundary conditions in the large-eddy simulation of high Reynolds number flow. Flow Turbulence Combustion 1999;63:269–91.
[92] Piomelli U, Balaras E. Wall-layer models for large-eddy simulation. Ann Rev Fluid Mech 2002;34:349–74.
[93] Balaras E, Benocci C, Piomelli U. Two-layer approximate boundary conditions for large-eddy simulations. AIAA J 1996;34:1111–9.
[94] Davidson L, Peng SH. Hybrid LES–RANS modelling: a one-equation sgs model combined with a k-ω model for predicting recirculating flows. Int J Numer Methods Fluids 2003;43(9):1003–18.
[95] Temmerman L, Hadžiabić M, Leschziner MA, Hanjalić K. A hybrid two-layer URANS–LES approach for large eddy simulation at high Reynolds numbers. Int J Heat Fluid Flow 2005;26:173–90.
[96] Yoshizawa A, Horiuti K. A statistically-derived subgrid-scale kinetic energy model for the large-eddy simulation of turbulent flows. J Phys Soc Jpn 1985; 54:2834–9.
[97] Hamba F. A hybrid RANS/LES simulation of turbulent channel flow. Theoret Comput Fluid Dyn 2003;16:387–403.
[98] Davidson L, Dahlström S. Hybrid LES-RANS: computation of the flow around a three-dimensional hill. In: Engineering turbulence modelling and experiments, vol. 6. Amsterdam: Elsevier; 2005.
[99] Yakhot V, Orszag SA. Renormalization group analysis of turbulence. 1. Basic theory. J Sci Comput 1986;1(1):3–51.
[100] DeLanghe C, Merci B, Dick E. Very large eddy simulation and RNG turbulence models. AIAA Paper 2001–3041; 2001.
[101] DeLanghe C, Merci B, Dick E. Hybrid RANS/LES modelling with an approximate renormalization group. I: model development. J Turbulence 2005;6(13):1–18.
[102] DeLanghe C, Merci B, Lodefier K, Dick E. Hybrid RANS/LES modelling with an approximate renormalization group II: applications. J Turbulence 2005; 6(13):1–16.
[103] Batten P, Goldberg U, Chakravarthy S. Sub-grid turbulence modelling for unsteady flow with acoustic resonance. AIAA Paper 2000–0473; 2000.
[104] Batten P, Goldberg U, Chakravarthy S. Interfacing statistical turbulence closures with large-eddy simulation. AIAA J 2004;42(3):485–92.
[105] Batten P, Goldberg U, Chakravarthy S. LNS—an approach towards embedded LES, AIAA Paper 2002–0427; 2002.
[106] Sergent E. Vers une méthodologie de couplage entre la simulation des grandes échelles et les modèles statistiques. PhD thesis, Ecole Centrale de Lyon; 2002.
[107] Sergent E, Bertoglio JP, Laurence D. Coupling between large-eddy simulation and Reynolds-averaged Navier–Stokes. In: Presentation at 3rd international workshop on direct and large eddy simulation, Munich, no written contribution; 2003.
[108] Mathey F, Cokljat D, Bertoglio JP, Sergent E. Specification of LES inlet boundary condition using vortex method. In: Hanjalić K, Nagano Y, Tummers M, editors. Turbulence Heat, and Mass Transfer, vol. 4. Begell House; 2003.
[109] Mathey F, Cokljat D. Zonal multi-domain RANS/LES simulation of airflow over the Ahmed body. In: Rodi W, Mulas M, editors. Engineering turbulence modelling and experiments. vol. 6. 2005; p. 647–56.
[110] Grinstein F. Special section: boundary conditions for LES. AIAA J 2004; 42(3):437–92.
[111] Lefebvre de Plinval-Salgues H. Implementation and evaluation of a method to generate turbulent inlet boundary conditions for a large eddy simulation. Internal Report, Institute for Hydromechanics, University of Karlsruhe; 2004.
[112] von Terzi DA, Rodi W, Fröhlich J. Scrutinizing velocity and pressure coupling conditions for LES with downstream RANS calculations. In: Peng S-H, Haase W, editors. Advances in hybrid RANS–LES modelling. Notes on numerical fluid mechanics and multidisciplinary design, vol. 97. Berlin: Springer; 2008. p. 107–16.
[113] Schlüter JU, Wu X, Kim S, Shankaran S, Alonso JJ, Pitsch H. A framework for coupling Reynolds-averaged with large-eddy simulations for gas turbine applications. J Fluids Eng 2005;127:806–15.
[114] von Terzi DA, Fröhlich J. Coupling conditions for LES with downstream RANS for prediction of incompressible turbulent flows. In: Proceedings of the 5th international symposium on turbulence and shear flow phenomena TSFP-5, vol. 2. Elsevier; 2007. p. 765–70.
[115] von Terzi DA, Fröhlich J. Zonal coupling of LES with downstream RANS calculations; 2008, in preparation.
[116] Moser RD, Kim J, Mansour NN. Direct numerical simulation of turbulent channel flow up to $Re_\tau = 590$. Phys Fluids 1999;11:943–5.
[117] Girimaji SS. Partially-averaged Navier–Stokes model for turbulence: a Reynolds-averaged Navier–Stokes to direct numerical simulation bridging method. J Appl Mech 2006;73:413–21.
[118] Rotta JC. Turbulente Strömungen. Stuttgart: Teubner; 1972.
[119] Menter FR, Egorov Y. Re-visiting the turbulent scale equation. In: Meier GEA, Sreenivasan KR, editors. IUTAM symposium on one hundred years of boundary layer research: proceedings of the IUTAM symposium held at DLR—Göttingen, Germany, August 12–14, 2004. Solid mechanics and its applications, vol. 129. Berlin: Springer; 2006. p. 279–90.
[120] Menter FR, Kuntz M, Bender R. A scale-adaptive simulation model for turbulent flow predictions. AIAA Paper 2003-0767; 2003.
[121] Egorov Y, Menter FR. Development and application of SST–SAS turbulence model in the DESIDER project. In: Peng S-H, Haase W, editors. Advances in hybrid RANS–LES modelling. Notes on numerical fluid mechanics and multidisciplinary design, vol. 97. Berlin: Springer; 2008. p. 261–70.
[122] Menter FR, Egorov Y, Rusch D. Steady and unsteady flow modelling using the $k-\sqrt{kl}$ model. In: Hanjalić K, Nagano Y, Jakirlić S, editors. Turbulence heat and mass transfer, vol. 5. Begell House; 2006. p. 403–5.
[123] Menter FR, Egorov Y. A scale-adaptive simulation model using two-equation models. AIAA Paper 2005-1095; 2005.
[124] Menter FR, Egorov Y. SAS turbulence modeling of technical flows. In: Lamballais E, Friedrich R, Geurts BJ, Métais O, editors. Direct and large-eddy simulation VI, Poitiers, September 12–14, 2005. Berlin: Springer; 2006. p. 687–94.
[125] Davidson L. Evaluation of the SST–SAS model: channel flow, asymmetric diffuser and axis-symmetric hill. In: European conference on computational fluid dynamics: ECCOMAS CFD; 2006.
[126] Davidson L, Dahlström S. Hybrid LES–RANS: computation of the flow around a three-dimensional hill. In: Rodi W, Mulas M, editors. Engineering turbulence modelling and measurements. vol. 6. 2005; p. 319–28.
[127] Medic G, Daeninck G, Templeton JA, Kalitzin G. A framework for near-wall RANS/LES coupling. In: Annual research briefs—2005, Center for Turbulence Research, Stanford University; 2005.
[128] Medic G, Templeton JA, Kalitzin G. A formulation for near-wall RANS/LES coupling. Int J Eng Sci 2006;44:1099–112.
[129] Brandt T, Hellsten A, von Terzi DA, Fröhlich J. Assessment of a hybrid LES–RANS concept based on eddy-viscosity reduction using resolved Reynolds stresses. In: Proceedings of the 5th congress on computational methods in applied sciences and engineering, ECCOMAS 2008, June 30–July 5, Venice, Italy; 2008, to appear.